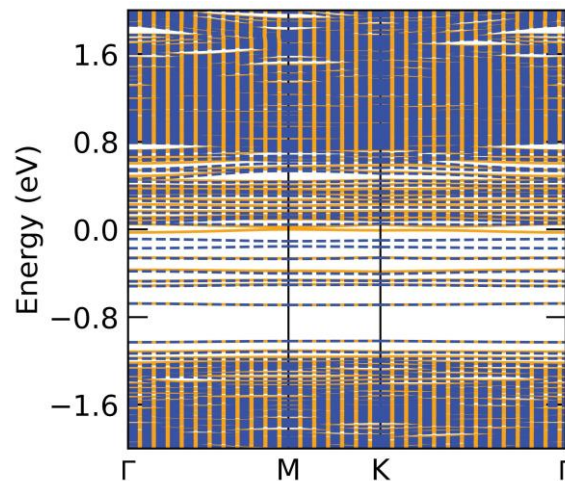**MASTER THESIS NO. 2022:22**

College of Science

Department of Physics

BANDGAP TUNING OF MoSe$_2$ AND WSe$_2$ MONOLAYERS THROUGH ALLOYING AND SUBSTITUTION: AN AB INITIO STUDY

Shahida Maqsood

March 2022

United Arab Emirates University

College of Science

Department of Physics

BANDGAP TUNING OF MoSe$_2$ AND WSe$_2$ MONOLAYERS THROUGH ALLOYING AND SUBSTITUTION: AN AB INITIO STUDY

Shahida Maqsood

This thesis is submitted in partial fulfilment of the requirements for the degree of Master of Science in Physics

Under the Supervision of Professor Noureddine Amrane

March 2022

Declaration of Original Work

I, Shahida Maqsood, the undersigned, a graduate student at the United Arab Emirates University (UAEU), and the author of this thesis entitled "*Bandgap Tuning of* $MoSe_2$ *and* WSe_2 *Monolayers Through Alloying and Substitution: An Ab Initio Study*", hereby, solemnly declare that this thesis is my original research work that has been done and prepared by me under the supervision of Professor Noureddine Amrane, in the College of Science at UAEU. This work has not previously formed the basis for the award of any academic degree, diploma or a similar title at this or any other university. Any materials borrowed from other sources (whether published or unpublished) and relied upon or included in my thesis have been properly cited and acknowledged in accordance with appropriate academic conventions. I further declare that there is no potential conflict of interest with respect to the research, data collection, authorship, presentation and/or publication of this thesis.

Student's Signature: _____   Date: 22-03-2022

Advisory Committee

1) Advisor: Noureddine Amrane

Title: Professor

Department of Physics

College of Science

2) Co-Advisor: Maamar Benkraouda

Title: Professor

Department of Physics

College of Science

Approval of the Master Thesis

This Master Thesis is approved by the following Examining Committee Members:

1) Advisor (Committee Chair): Noureddine Amrane

   Title: Professor

   Department of Physics

   College of Science

   Signature _____   Date __18-04-2022__

2) Member: Saleh Thaker Mahmoud

   Title: Professor

   Department of Physics

   College of Science

   Signature _____   Date __18-04-2022__

3) Member (External Examiner): Mounir Kaidi

   Title: Professor

   Department of Physics

   Institution: University of Sharjah, UAE

   Signature _____   Date __18-04-2022__

This Master Thesis is accepted by:

Dean of the College of Science: Professor Maamar Benkarouda

Signature _Maamar Benkraouda_ Date June 21, 2022

Dean of the College of Graduate Studies: Professor Ali Al-Marzouqi

Signature _____Ali Hassan_____ Date __June 21, 2022__

Abstract

2D materials attracted considerable interest in the research community following the first report in 2004 on the preparation of graphene by simple micromechanical exfoliation of highly oriented pyrolytic graphite. For example, single-layer Molybdenum Di selenide ($MoSe_2$) and Tungsten Di selenide (WSe_2) transistors with on/off ratios of 108 and ultra-low standby power dissipation were demonstrated. Graphene electrodes have been used to develop fully transparent resistive memories to suppress unwanted surface effects that occur in oxide memory devices. Photodetectors based on $MoSe_2$ with few layers have shown excellent photodetection properties. Phototransistors based on WSe_2 monolayers exhibit photosensitivity up to 2200 AW, demonstrating the emerging applications of 2D materials for high-efficiency optoelectronic devices. In particular, the 2D monolayers of semiconducting transition metal dichalcogenides (TMDs) exhibit direct bandgaps and have intriguing optical properties suitable for optoelectronic applications in light-emitting diodes and photovoltaics. To realize highly efficient optoelectronic devices based on TMD monolayers, it is also essential to develop a strategy for tuning the bandgaps of TMD monolayers. A significant drawback of graphene is that it does not have a bandgap and is therefore not considered the best material for light-emitting devices. This drawback of graphene has severely limited its application in the electronics industry, where semiconductor materials are widely used. In contrast, single-layer TMDs such as WSe_2 and WSe_2 are direct bandgap semiconductors and show good light emission properties. In this work, density functional theory is used to perform systematic studies of layered $MoSe_2$ and WSe_2. Theoretically, we transition metals Rh and Ru to perform planned studies of layered $MoSe_2$ and WSe_2 via substitutional doping and vacancies to find suitable dopants that can effectively improve or change these materials' electrical and magnetic properties. VASP is used as a theoretical, computational tool to determine the electronic and magnetic properties of untreated, defected, and doped $MoSe_2$ and WSe_2. Vacancy creation and doping reduced bandgap values as vacancies and doping concentrations increased linearly. Vacancy creation and doping reduced bandgap values as vacancies and doping concentrations increased linearly. Calculations of the energies of formation suggest that the doped system is thermodynamically more stable than the system with vacancies. The results obtained show that the Ru doped system

has lower formation energies than the Rh. This study shows that both $MoSe_2$ and WSe_2 acquire a semi-metallic character. Both doped and vacancy generated systems bring magnetism to $MoSe_2$ and WSe_2, and the highest value of total magnetic moment found is 12 μ_B for tri-vacancies in $MoSe_2$. This research shows that both vacancy generation and doping are practical tools for future scientific applications based on WSe_2 and $MoSe_2$.

Keywords: Bandgap, $MoSe_2$, WSe_2, DFT, Doping, Monolayer, Point Defects, Transition Metal, VASP, 2D Material.

Title and Abstract (in Arabic)

ضبط فجوة النطاق للطبقات الأحادية للموليبدينوم دايسيلينيد ($MoSe_2$) و للتنغستن دايسلينيد (WSe_2) من خلال السبائك والاستبدال: دراسة أولية

الملخص

اكتسبت المواد ثنائية الأبعاد اهتماما كبيرا بين مجتمع البحث بعد التقرير الأول عن إعداد الجرافين عن طريق تقشير ميكروميكانيكي بسيط للجرافيت الحراري عالي التوجه في عام 2004.على سبيل المثال، تم إثبات ترانزستورات الموليبديوم دايسيلينيد ($MoSe_2$) والتنغستن دايسلينيد (WSe_2) أحادية الطبقة بنسب تشغيل / إيقاف 108 وتبديد الطاقة الاحتياطية المنخفضة للغاية. تم تطبيق أقطاب الجرافين الكهربائية في تطوير ذاكرة مقاومة شفافة تماما لقمع التأثيرات السطحية غير المرغوب فيها الموجودة في أجهزة ذاكرة الأكسيد. أظهرت أجهزة الكشف الضوئي القائمة على $MoSe_2$ ذات الطبقات القليلة خصائص ممتازة للكشف عن الضوء. كما تم الإبلاغ عن أن ترانزستورات الصور القائمة على WSe_2 أحادية الطبقة تظهر مسؤولية ضوئية تصل إلى 2200 AW مما يدل على التطبيقات الناشئة للمواد ثنائية الأبعاد للأجهزة الإلكترونية البصرية عالية الكفاءة. على وجه الخصوص، تحتوي الطبقات الأحادية 2D من ثنائي الكالكوجينيدات المعدنية الانتقالية شبه الموصلة (TMDs) على فجوات نطاق مباشرة، وتمتلك خصائص بصرية مثيرة للاهتمام مناسبة للتطبيقات الإلكترونية البصرية في الثنائيات الباعثة للضوء والخلايا الكهروضوئية. لتحقيق الأجهزة الإلكترونية الضوئية عالية الكفاءة القائمة على الطبقات الأحادية TMDs، من المهم أيضا تطوير استراتيجية لضبط فجوات النطاق للطبقات الأحادية TMDs. أحد العيوب الرئيسية في الجرافين هو أنه يفتقر إلى وجود فجوة في النطاق، وبالتالي فهو لا يعتبر مادة مثالية لأجهزة الانبعاثات الخفيفة، وقد قلل من تطبيقه في الصناعة الإلكترونية حيث قد تكون مواد أشباه الموصلات ذات فائدة كبيرة. على العكس من ذلك، تعتبر TMDs أحادية الطبقة مثلWSe_2 وWSe_2 أشباه موصلات فجوة النطاق المباشر وتظهر خصائص جيدة باعث للضوء في هذه الأطروحة، يتم استخدام نظرية الكثافة الوظيفية لإجراء دراسات منهجية لـ $MoSe_2$ وWSe_2 الطبقات. من الناحية النظرية، نأخذ الفلزات الانتقالية Rh وRu لإجراء دراسات مخططة لـ $MoSe_2$ وWSe_2 عبر المنشطات البديلة وعيوب الشواغر بهدف تحديد المنشطات المناسبة التي يمكن أن تعزز أو تعدل بشكل فعال الخصائص الكهربائية والمغناطيسية لهذه المواد. يستخدم VASP كأداة حسابية نظرية للعثور على الخصائص الإلكترونية والمغناطيسية لـ $MoSe_2$

وWSe₂ البكر والمعيب والمنشط. ومن الثابت أن كلا من خلق الشواغر والمنشطات، يقلل خطيا من قيم فجوة النطاق مع زيادة عدد الشواغر وتركيزات المنشطات. يشير حساب طاقات التكوين إلى أن النظام المنشط أكثر استقرارا من الناحية الديناميكية الحرارية من النظام الذي يحتوي على وظائف شاغرة. تشير نتائجنا إلى أن نظام Ru doped يحتوي على طاقات تكوين أقل من Rh doped . يظهر هذا البحث أن الحرف نصف المعدني يتم تحفيزه في MoSe₂ وWSe₂ بكلتا الطريقتين المستخدمتين. كل من الأنظمة التي تم إنشاؤها بالمنشطات والشواغر تجلب المغناطيسية إلى MoSe₂ وWSe₂ وأعلى قيمة لإجمالي العزم المغناطيسي الموجود هي 12 ميكرو B للشواغر الثلاثية في MoSe₂.يظهر هذا البحث أن إنشاء الوظائف الشاغرة والمنشطات، كلاهما أداة فعالة لبناء تطبيقات علمية قائمة على WSe₂ وMoSe₂ في المستقبل.

مفاهيم البحث الرئيسية: المعادن الانتقالية، الموليبديوم دايسيلينيد، التنغستن دايسلينيد، فجوة النطاق، الطبقة الأحادية، مادة 2D، المنشطات، عيوب النقاط.

Acknowledgements

Dedication

To my beloved parents and family

Table of Contents

List of Tables

List of Figures

List of Abbreviations

CBM	Conduction Band Minima
DFT	Density Function Theory
DOS	Density of States
GGA	Generalized Gradient Approximation
HF	Hartree-Fock
PAW	Projector Augmented Wave
PBE	Perdew–Burke–Ernzerhof
PDOS	Projected Density of States
PL	Photoluminescence
TM	Transition Metal
TMDs	Transition Metal Dichalcogenide
VASP	Vienna Initio Simulation Package
VBM	Valence Band Maximum

Chapter 1: Introduction

This chapter supplies the foundation for the research to be conducted. The background and goal of this study will be discussed extensively. An overview of the earlier work will also be provided to explore the topic's scope further.

1.1 Overview

Transition metal dichalcogenide monolayers are very favourable materials for many applications in electronics and optoelectronics and have been extensively studied in the recent past, both experimentally and theoretically. In 2004, a new science for the study of 2D materials emerged with the discovery of graphene (Novoselov et al., 2004) Graphene is a single layer of carbon atoms structured in a honeycomb with special electronic properties (Neto et al., 2009). Its band structure shows that it has no direct bandgap, which makes it difficult for future photoelectronic devices. To address these issues, the few TMD layers provide a good opportunity for such efforts in future research. $MoSe_2$ and WSe_2 are two of these promising compounds that have an indirect bandgap that can later be tuned to the visible region of the solar spectrum.

This work aims to tune the bandgap of 2D layer transition metals (LTMD) to improve their application for photosensitive devices. LTMD is a class of graphene-like materials that are widely studied due to their various properties such as carrier mobility, flexibility, and optical properties that qualify them as suitable candidates for devices. The structure of LTMDs is unique and has the formula MX2 (where M is a transition metal and X is a chalcogen), with the two connected by covalent bonds in an octahedron. Recently, two-dimensional MX2 (M=Mo, W; X=S, Se, Te) thin films have been developed, exhibiting unique optical and electrical properties different from

their bulk counterparts due to the direct bandgap transition (Cheiwchanchamnangij & Lambrecht, 2012; Jin et al., 2013; Li et al., 2014), with large nonlinear optical responses offering them new opportunities as monolayer materials.

Recently, many studies have been conducted to modulate the physical properties such as defects, chemical absorption, and doping of single-layer LTMDs. Doping is very effective to tune bandgaps and electronic structures. Doping with transition metals (TM) has been used very successfully, e.g., $MoSe_2$ is converted into a semimetal by substitution of Co, V, Mn, Fe, and Ni (Wang et al., 2016). Many recent pieces of research have shown and tested that the substitution can improve the electronic and optical properties of monolayer TMD and provide new promising applications. Therefore, changing the bandgap is an effective way to improve the electronic and magnetic properties of TMD. $MoSe_2$, WSe_2 is a promising representative of TMDs, which is characterised by a direct bandgap, high photosensitivity, and thermal stability due to their electronic and magnetic properties that can be tuned by creating vacancies and doping suitable elements. Rh and Ru are some rare earth and transition metal elements that have been used for substitutional doping in this research (Payne et al., 1992).

1.2 Statement of the Problem

In this work, density functional theory is used to perform systematic studies of layered $MoSe_2$ and WSe_2. Theoretically, we take transition metals and rare earth metals to perform systematic studies of layered $MoSe_2$ by substitution doping and vacancy creation. In addition, the search for their effects on the layered compounds with different thicknesses is extended to a wide range of concentrations. The goal is to

successfully achieve the bandgap tunability of layered $MoSe_2$ and WSe_2 so that we can predict and design the systems with high performance.

1.2.1 Theoretical Modelling

All computational studies are performed using the Vienna Initio Simulation Package (VASP), with ion potentials including the effect of core electrons described by the Projector Augmented Wave (PAW) method. Brillouin zone integration is performed on well-converged gamma k-point grids. A plane wave energy limit of 500 eV is used in all calculations. All structures are geometrically relaxed until the total force on each ion is reduced to less than 0.01 eV/Å.

1.2.2 Choice of the Computational Framework

In choosing the computational framework, we note that standard density functional theory (DFT), using the Generalized Gradient Approximation (GGA) for the exchange-correlation functional (XC), calculates the electronic and magnetic properties of $MoSe_2$ and WSe_2. Searching for the effects of transition and rare earth metals on $MoSe_2$ and WSe_2 monolayers. We will investigate the effects of a wide range of concentrations of transition and rare earth metals on $MoSe_2$ and WSe_2 thin films, where Rh and Ru atoms are introduced as dopants into the Mo lattice sites, causing the transition from deep to shallow impurity states in $MoSe_2$ and WSe_2 monolayers.

1.2.3 Research Hypotheses

The bandgaps of $MoSe_2$ and WSe_2 with few layers are close to 2 eV, which is not yet very efficient for photovoltaic applications. It is important to develop a doping strategy to reduce the bandgap and thus be able to use a significant part of the solar spectrum. Therefore, we introduce transition metals, including 3d and 4d elements, in $MoSe_2$ and

WSe$_2$ to find suitable transition metals that can effectively reduce the bandgap and extend the optical absorption to the visible range and even the infrared range.

1.2.4 Impact of this Research Work

The outcomes of the proposed research will contribute directly to the social goals articulated in the Emirates Economic Vision 2030. The United Arab Emirates has taken a big move by creating the Mubadala technology company and Semiconductor Research Corporation (SRC). We believe that our research project will be beneficial to the University and the electronics industry in the UAE.

1.3 Pure TMD's Structural and Electronic Properties

TMDs are layered materials with strong in-plane bonds but weak Vander-Waals forces. Their chemical formula is MX2, where M is a transition metal and X is chalcogen atoms. Transition elements (IV-VI) include Mo, W, V, Nb, TI, etc. and chalcogens include S, Se, and Te. (X-M-X) represents a monolayer of TMD. There is a strong bond between the atomic planes M and X. The studied TMDs MoSe$_2$ and WSe$_2$ are both semiconductors with hexagonal structures and belong to space group P6. A pure primitive cell of a TMD has 2 metal atoms and 4 chalcogen atoms.

Experimental results show bandgaps matching the solar spectrum and were obtained by Kam and Parkinson (1982). The bandgaps of MoS$_2$ and WS$_2$ are 1.23 eV and 1.35 eV correspondingly (Kam & Parkinson, 1982). Layered TMD has always been of interest for bulk materials. The band structures were calculated using the augmented spherical wave method. MoSe$_2$ and WSe$_2$ are both indirect semiconductors with maxima of the v-zone at the Γ-point and minima of the c-zone at the K-point, as shown in Figure 1 (Coehoorn et al., 1987).
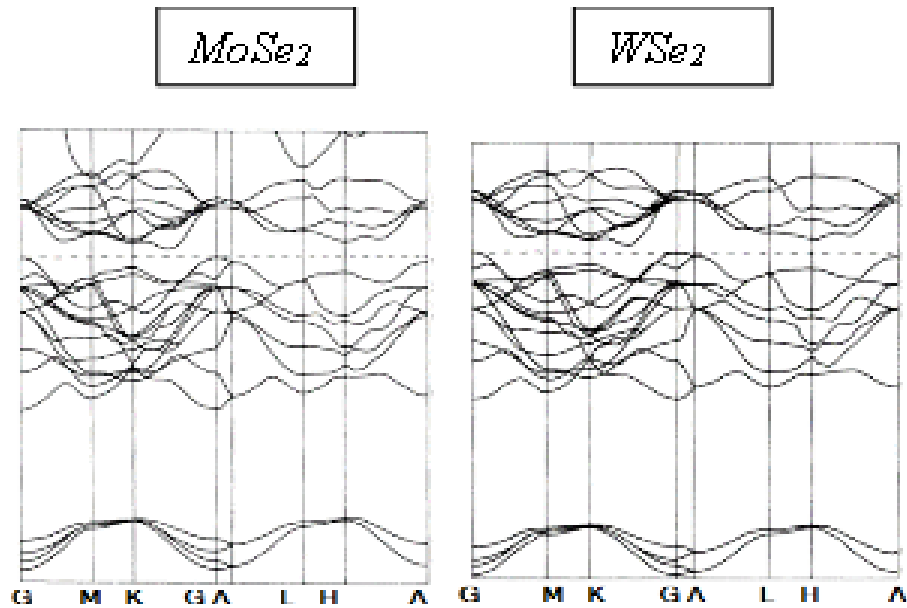
Figure 1: Scalar Relativistic Band Structures of MoSe$_2$ Bulk. Adapted from (Coehoorn et al., 1987)

1.3.1 The Density Functional Theory (DFT)

In theoretical physics, it was a real problem to determine the structure of a system with many electrons. In a semiconductor, nuclei and electrons are the two essential entities, and their interaction is significant. The nucleus is heavier than the electron; therefore, in the Born-Oppenheimer approximation, the nuclei are assumed not to move, and the electrons move at an ineffective potential. The nonrelativistic, time-independent Schrödinger equation explains systems. There are many salient features of DFT, including the Hohenberg-Kohn theorem. The standard Hamiltonian describing N-body particles can be written as:

$$\widehat{H} = \widehat{T} + V_{ext} + W \qquad\qquad \text{(Equation 1.1)}$$

Where $\widehat{T}$ is the kinetic energy operator, V_{ext} is the time-independent potential and $\widehat{W}$ is the term for particle interactions (Eberhard & Dreizler, 2011). Solving Schrödinger equation gives many bodies Eigen states Ψ_k ⟩.

$$\langle \widehat{H} | \Psi_k \rangle = | E_k | \Psi_k \rangle \qquad \text{(Equation 1.2)}$$

Among the solutions of the above equation, $|\Psi_0\rangle$ is described as a ground state.

1.3.2 LDA and GGA Approximations of Exchange-Correlation Functions

Many approximations of the above functions are used because the correct form is not precisely known. The LDA approximates the local density. The exchange-correlation potential is approximated at each point in space as a known xc potential from the heterogeneous electron gas for the electron density observed in space (Sholl & Steckel, 2011). Another approximation developed after LDA is the Generalized Density Approximation (GGA), which considers the density and its local gradient. There are several ways to implement LDA and GGA, but the Perdew-Burke-Ernzerhof functional (PBE) and the Perdew-Wang functional (PW91) are the most used GGA functions for computations with solids. We will use the implementation of PBE-GGA for calculations.

1.3.3 The Bandgap Energy

The least amount of energy is required for an electron to break free from the valance band and jump into the conduction band. The weakest bound electron belongs to the highest filled valance band, and the $(N+1)_{th}$ electron belongs to the lowest empty band, i.e., the conduction band of the neutral system. The equation for calculating the band-gap energy can be written as follows:

$$\Delta s = \varepsilon_{N+1} - \epsilon_N \qquad \text{(Equation 1.3)}$$

1.3.4 Supercell Concept

Density functional theory (DFT) is applied to the system under consideration to calculate various parameters, including the bandgap. First, the volume of the crystal

must be defined and the positions of the atoms within the volume should also be specified. Then vectors can be set up in both directions that define the crystal. The vectors and atomic positions within the specified cell are called the supercell. This is the most basic basis for the calculations of DFT. A primitive cell is a supercell with a minimum number of atoms required to define a crystal structure.

1.4 Relevant Literature Review

The interest in two-dimensional (2D) semiconductors is mainly fuelled by the highly successful miniaturisation of Si-based electronic devices, which enable higher packing density, faster-switching speed and lower power dissipation (Vargas-Bernal, 2019; Weng et al., 2018). Recently discovered 2D materials have attracted the interest of researchers due to their promising applications in the optical and electrical industries. Graphene has ushered in a new era in photonics and optoelectronics with its high optical transparency (97.7% transmittance in the visible spectrum), good thermal conductivity at room temperature (3×10^3 W/mK) and exceptional mechanical strength, i.e., Young's modulus of 1.1TPa (Sang et al., 2019; Sung et al., 2019). Due to these properties, graphene is at the top of the list as a candidate for transparent electrodes, energy storage devices and solar cells. These outstanding properties have increased the demand for more research in 2D layered materials. However, a significant drawback of graphene is its lack of a bandgap (Rout et al., 2019), which is why it is not considered an optimal material for light-emitting devices and minimises its application in the electronics industry, where semiconductor materials could be of great use.

Molybdenum selenide and tungsten Di selenide appear to be a promising class of materials for next-generation electronics. It is the only 2D material discovered so far

that has an inherent bandgap. With this property, they pave the way for the development of a whole new domain of electronic devices and materials that can be used in heterostructures with other 2D layered materials to complement each other. $MoSe_2$ and WSe_2 exhibit good electrical and transport properties (Daukiya et al., 2019; Habib et al., 2019; Liu et al., 2019) and are chemically and thermally stable, transparent, flexible, and relatively inexpensive, making this material an excellent overall candidate for a variety of electronic and optoelectronic applications. The 2D form of the material was first discovered in 2011 when scientists succeeded in fabricating a transistor from this new material (Donaldson, 2019).

Many recent reports have shown that $MoSe_2$ and WSe_2 can be synthesised cost-effectively and can actively absorb much more irradiated energy from the solar spectrum than conventional solar cells made of organic materials and silicon (Jia, 2019; Morgan et al., 2019). Undoubtedly, it will help solve the environmental and energy problems in the UAE and even worldwide. Recently, many researchers used density functional theory (DFT) in investigating the potential effects of the adsorption of metals on $MoSe_2$. Monolayers of 2D $MoSe_2$ were doped with metals such as Pd, Pt, Cu, Ag, Au, and Zn, resulting in stable adsorption for all except Zn. In addition, magnetic properties were introduced in Cu, Ag and Au systems. LEDs such as $MoSe_2$ are promising as their bandgap can be manipulated by adding certain elements that can shift them from an indirect bandgap to a direct one.

The band structure of $MoSe_2$ has changed from metallic, semi-metallic to semiconducting behaviour upon the adsorption of certain metals, leading to magnetic moments. It suggests the Production of nano-electronic devices made of doped $MoSe_2$ or MoS_2 (Huang et al., 2017). Although the structural properties of graphene are near

to TMDs such as $MoSe_2$, WSe_2, WS_2, and MoS_2, they have a bandgap from 1-2 eV (Kumar & Ahluwalia, 2012), which makes them a perfect candidate for future electronic devices. Currently, they are applied to field-effect transistors (Garnier et al., 1994; Tsumura et al., 1986), optoelectronic devices and transducers (Li et al., 2006).

In recent years, TMDs have been extensively studied and focused on their various properties, including the ability of $MoSe_2$ to change the bandgap. WSe_2 has been considered for use in low-cost thin-film solar cells due to its small bandgap and high absorption coefficient. Possible applications include transistors, photovoltaics, and light-emitting devices. The Mn-doped monolayer of $MoSe_2$ has been studied using DFT and the results represent a promising new area of magnetic semiconductors. Similar studies were carried out with WS_2, whose bandgap was raised from an indirect bandgap of 1.3 eV to 2 eV after the fabrication of single layers.

Li et al. (2016) observed that one X doped WS_2 is nonmagnetic, while 2X doped results in magnetic moments. A few years back, multiple methods were used to change the physical properties of layered TMDs; they were used for applications such as defects (Li et al., 2013), doping (Tongay et al., 2013), strain engineering (Zhou et al., 2013). $MoSe_2$ single layer TMD has been widely studied because of its good physical properties such as bandgap (Kumar & Schwingenschlogl, 2015), and photoluminescence (Tonndorf et al., 2013) and interesting thermal stability (Tongay et al., 2012).

In recent years, researchers have also investigated how strains or defects in the monolayer of WSe_2 can affect its magnetic properties. It has been proven that two W atoms and one W atom and three nearby Se atom pairs induce magnetic moments in the monolayer of WSe_2. WSe_2 with defects can exhibit different electronic properties

depending on the tensile stress. Previous studies have shown that point defects and vacancy defects induce magnetism in graphene and $MoSe_2$ monolayers. These 2D materials show tremendous ability to handle strain due to their plastic deformability. It has been studied that all vacancy defects change the electronic properties of WSe_2, while certain vacancies introduce magnetic moments into the material. The WSe_2 monolayer with W vacancy transforms from a non- magnetic material into a magnetic one (Zhang et al., 2019).

Zhang et al. (2020) also revealed that the 3d transition metals Mn, Fe, Co, and Ni, when doped into a $MoSe_2$ monolayer, were found to enhance the electronic transport properties by adding flat impurity bands within the bandgap. It was discovered that Co doping makes WSe_2 a semimetal and substitution of certain metals V, Mn, Fe, Co, and Ni brings out the metallic behaviour. All added metallic impurities were shown to favour the energetically doped systems under Se-rich conditions. It was found that all TM impurities cause some lattice distortion. The 3d orbital of the metallic impurities improves the electron transport properties, and the TM doping is a possibility to fabricate $MoSe_2$-based nanodevices.

Wang et al. (2017) have investigated TMD by doping them with various metals and non-metals. The results laid the foundation for the study of modulation of electronic, magnetic and transport properties of monolayers TMD. They found out that doping of non-metals into $MoSe_2$ is energetically favourable compared to Se vacancies. Likewise, even valance electron doping always results in p-type material. In contrast, odd valance electron doping results in either p or n-type materials, which provides an insight into tuning the bandgap and studying the field of optoelectronics and electronics.

Chapter 2: Methods

In this chapter, the method of research will be discussed extensively with the theoretical background involved. VASP is the computational code used to find the electronic and magnetic properties of WSe_2 and WSe_2.Many bodies' problems will be talked over to explore density functional theory. Two methods of bandgap tuning i.e., vacancy creation and substitutional doping will be discussed in detail.

2.1 The Many-Body Problem

All the materials consist of many electrons and nuclei, and they interact with each other which describes the properties of a material. Since we are discussing the electromagnetic interactions at the atomic level, we will apply quantum mechanics. The basic equation that explains the quantum mechanical system is the many-body Schrodinger equation which is given by:

$$H\psi = E\psi \qquad\qquad (Equation\ 2.1)$$

where H is the Hamiltonian operator, Ψ is the wave function and E is the energy. This Hamiltonian can be divided into five terms.

$$H = T_e + T_I + V_{ee} + V_{II} + V_{eI} \qquad\qquad (Equation\ 2.2)$$

Where T_e and T_I describe the kinetic energies of electrons and ions respectively and V_{ee}, V_{II}, and V_{eI} are the potential energy operators describing the electron-electron, the ion-ion, and the electron -ion coulomb interaction, respectively.

The wave function Ψ depends upon the ionic and electronic degree of freedom (r_i, R_I) and the above equation can be written as:

$$(\mathrm{T_e} + T_I + V_{ee} + V_{II} + V_{eI})\psi(r_i, R_I) = E\psi(r_i, R_I) \qquad \text{(Equation 2.3)}$$

The solution of Equation 2.3 gives the properties of the system. Since the solution

holds too many terms it is necessary to apply approximations. The first approximation

is Born-Oppenheimer (BO) approximation (Born & Oppenheimer, 1927). Since the

mass of the nuclei is many times more than an electron so electron moves faster and

hence, we can ignore the T_I term in Equation 2.3. Even though the nuclei are not

moving particles, finding the solution to the above equation is not easy as many

electrons are interacting with each other and along with the stationary nuclei. Also, the

wave function must be antisymmetric given the fermion nature of electrons. Hence the

solution to Equation 2.2 will be found by some approximations which will be

explained systematically in the following methods.

2.1.1 Born-Oppenheimer Approximation

According to this approximation, the nucleus is more massive than the electron, hence

the electrons can move faster as compared to the nuclei. To make the many bodies

problem less complicated, we can separate the terms in the Schrodinger equation for

electrons and nuclei. It means the dynamics of atomic nuclei and electrons are

separated so this Hamiltonian can be written as

$$H = H_e + H_n + H_{e-n} \qquad \text{(Equation 2.4)}$$

So, while using the BO approximation we freeze the nucleus positions and calculate

the wave function 'Ψ' and energy 'E' of the i_{th} electron and treat the system as many

one-electron problems.

2.1.2 Hartree Approximation

The total Hamiltonian is approximated as a sum of one-electron operators and the wave function as a product of eigenvectors of those operators.

$$\psi(r_1, r_2, r_3, \ldots \ldots) = \psi(r_1)\psi(r_2)\psi(r_3) \ldots \ldots \ldots \qquad \text{(Equation 2.5)}$$

2.1.3 Hartree-Fock Approximation

In 1924, the Hartree approximation was introduced to simplify the above Schrodinger equation and the wave function Ψ is considered as the product of the single independent electron wave function as given above in Equation 2.5 (Hartree, 1928). Hence the problem is reduced to a single independent particle Schrodinger equation. The new equation is

$$\left[T_e + V_{eff}\right]\Psi_i(r) = \varepsilon_i \, \Psi_i(r) \qquad \text{(Equation 2.6)}$$

where $\varepsilon_i(r)$ is the i_{th} electron energy eigen value. $T_è$ is the one-electron kinetic energy and V_{eff} is the effective potential. The electron density is given by

$$n_j(r) = \left|\Psi(r_j)\right|^2 \qquad \text{(Equation 2.7)}$$

Hartree approximation had a drawback in that it considered electrons as distinguishable particles while they are fermions and interchanging two electrons with each other changes the function. In 1930, Fock produced the improvement by assuming that the wave function is antisymmetric which obeys Pauli exclusion Principle. It says that two electrons with the same spin cannot occupy the same quantum state. He introduced slater determinant. HF did not account for the changes in the large systems as the number of electrons needed to form the basis functions is huge. It also did not cover the correlations of the many bodies system. It could not explain the characteristics of homogeneous gas and metals. Hence a more correct

beyond HF was needed which could consider the correlation effects into account and give the material properties more precisely. DFT is the most current way to include both exchange and correlational effects.

2.2 Density Functional Theory (DFT)

DFT is a computational quantum mechanical modelling method used in physics, chemistry, & material science to investigate the electronic structure (ground state) of many-body systems (Kohanoff et al., 2003; Payne et al., 1992). This theory provides a solution to many electrons system using functionals. In DFT instead of wave functions, we consider density functional. We can solve the Schrodinger equation for a single electron body but for many bodies problem, we must add many terms and approximations into the Schrodinger equation to make it work. Following is the Schrodinger equation for a single electron.

$$\hat{H} = \frac{\hat{p}^2}{2m} + U(\hat{r}) \qquad \text{(Equation 2.8)}$$

The many bodies Hamiltonian can be written as

$$\hat{H} = \sum_i \frac{\hat{p}_i^2}{2m} + \sum_i U(\hat{r}_i) + \frac{1}{2} \sum_{i \ne j} V(\hat{r}_i - \hat{r}_j) + three\ body\ terms + \dots$$

$$\text{(Equation 2.9)}$$

In DFT we do not solve the wave function, but we focus on electron density ρ (x, y, z). This theory is an efficient tool to work out many complicated analyses supplying faster computational methods which are closed to experimental results.

$$\hat{H}\Psi\{(r_i, R_I\} = E\ \Psi\{\widehat{(r_i)}, \widehat{(R_I)}\} \qquad \text{(Equation 2.10)}$$

$$\hat{H} = \hat{T} + \hat{V}_{Coloumb} \qquad \text{(Equation 2.11)}$$

It supplies a swift code for electronic structure calculations. According to the HF method, the solution to the Schrodinger equation (Kohn & Sham, 1965) can be written as

$$V_{ext}(r, R) \rightarrow \psi(r, R) \, and \, E(R) \rightarrow Properties \qquad \text{(Equation 2.12)}$$

In the HF method, it starts with a 3N dimension potential which is a function of electron position 'r' and after formulating the Hamiltonian it leads to finding the wave function and energy. Whereas DFT focuses on the electron density rather than many bodies' wave function Ψ (r). This reduces the problem from 3N dimensions to three dimensions.

$$N(r) \rightarrow \psi(r, R) \, and \, E(R) \Rightarrow Properties \qquad \text{(Equation 2.13)}$$

DFT is based on two main theorems of Hohenberg and Kohn. (Hohenberg & Kohn, 1964). The first theorem is about ground-state electron density n(r) which determines the external potential (Bhimanapati et al., 2015; Hohenberg & Kohn, 1964). As of consequence of the two theorems, we can infer that ground state energy is also a function of the ground state density that is if ground state density is known, the ground state energy is a function of the density.

$$E_0 = E[n(r)] \qquad \text{(Equation 2.14)}$$

The 2nd Hohenberg Kohn theorem Confirms that the energy functional E[n(r)] minimum value gives the exact ground state energy and the electron density n(r) which minimizes this functional is the exact ground state density n_0(r).

2.2.1 Kohn-Shams Equations

In the preceding section, it is discussed that the ground state energy is a function of the electron density, (Kohn & Sham, 1965) but the exact nature of this function is unknown. It was a gigantic task for the success of the DFT. In 1965, the DFT started its journey of success due to the KS theory (Kohn & Sham, 1965). The main idea is to replace the many-body problem with an auxiliary system that can be approached with ease. The KS theory assumes that the ground state density of the tedious interacting system is the same as the non-interacting electrons moving in a mean-field way.

2.2.2 The Exchange –Correlational Energy Functional

As discussed in the earlier section, the KS equations mapped the many-body problem into a set of independent single particles equations. Nevertheless, the KS equations continue to be unresolved until we exactly define the exchange correlational functional E_{xc} [n(r)] in the following equation.

$$E[n(r)] = T_s[n(r)] + E_{Hartree}n[(r)] + E_{xc}[n(r)] + \int V_{ext}\, n(r)\, dr^3$$

(Equation 2.15)

The exact expression is not known exactly but estimation is applied. The many-body Hamiltonian can be written as if the non-interacting system and fully interacting system can be connected through a coupling constant λ (Born & Oppenheimer, 1927), (M Santhosh et al., 2020).

$$H_\lambda = \lambda V_{ee} + \lambda V_{ext}{}^\lambda$$
(Equation 2.16)

where λ=1 relates to the case of a noninteracting system and λ=1 is the original interacting one.

The standard methods for the exchange correlational function in DFT are LDA and GGA. These functional underestimates the bandgap of the system, hence the hybrid functional is applied to enhance precision.

2.2.3 Applications of DFT

There are many DFT packages like VASP, Quantum Expresso, ABINIT, SIESTA, and WIEN2k which make computations easy and faster including electron density functions, molecular geometries, and energy changes, dipole moments, vibrational frequencies, entropies and many more. There are many applications of DFT in material science to predict complex systems at an atomic scale. It is a quantum mechanical model which helps in computations of the electronic structure of atoms. They have been widely used very successfully in Physics and chemistry since 1970.

2.3 Research Design

Spin polarization Density Functional Theory (DFT) calculations are used along with (Projector Augmented Wave) PAW as implemented into VASP (Vienna Ab Initio Simulation Package) (Kohn & Sham, 1965). The GGA (Generalized Gradient Approximation) was used to describe the electron exchange-correlation effects in the form of Perdew-Burke- Ernzerhof (PBE) (Hohenberg & Kohn, 1964). Energy cut-off for the plane-wave expansion was established at 400 eV and the Brillouin-Zone integrations were carried out by the Gamma-cantered scheme with a 3x3x1 k-point grid (Bhimanapati et al., 2015). A vacuum spacing of 25 A was implemented to avoid artificial interactions between neighbouring super cells of $MoSe_2$ and WSe_2 as well. The two compounds will be subjected to bandgap tuning and will be studied for suitable dopants and the effects of vacancy creation on the bandgap.

2.3.1 Vienna ab initio Simulation Package (VASP)

VASP is a computer simulation package that can calculate atomic structure, optical and electronic properties etc. of the materials using the first Principal-theory. It calculates the approximate solution of many bodies Schrodinger equation using DFT, Kohn-Sham equations and other approximations like LDA, GGA and hybrid functionals. While using VASP, the fundamental quantities like electron charge density, one-electron orbitals, and local potentials are expressed in terms of plane-wave basis set. The interactions between electrons and ions are explained by ultrasoft pseudopotentials, or the Projector-Augmented-Wave method (PAW).

2.4 Calculation Setup Outline

All the calculations for the structural and electronic properties of the studies on Transition Metal Dichalcogenides (TMD) monolayers i.e., $MoSe_2$ and WSe_2 will use the parameters listed in Table 1.

Table 1: General Calculation Parameter

Parameter	Value
Kinetic energy cutoff (in eV).	400 eV ($MoSe_2$), 400 eV (WSe_2)
Mesh of k points	5 x 5 x 1
Inter layer distance for monolayers	20˚A

2.5 Structural Properties of $MoSe_2$ and WSe_2 Monolayers

This section will lay out the effects of the theoretical study of the structure and electronic properties of the $MoSe_2$ and WSe_2monolayers. In the beginning, the convergence test will be conducted for the cut-off kinetic energy and k-points sampling. Then, Relaxation calculations for the relaxed structure are performed to find

out the optimized lattice constant' a' for the mono layers. Finally, electronic properties of the TMD monolayers have been performed which include the band structure and Density of States (DOS).

For structural information of the chosen TMDs, the symmetry, space group, bond length lattice constant and atomic positions are significant. TMDs like $MoSe_2$ and WSe_2, are hexagonal in symmetry with space group P63/MMC. The TMDs monolayer (1L) has three atomic planes when two Chalcogens (Se) atoms sandwich with the metals (Mo, W) atoms. A monolayer primitive cell of TMDs will have 3 atoms, 1 metal and 2 Chalcogens. The structure of the monolayer TMDs is defined by the lattice constant a and c where c is the inter layer distance.

VASP is used to calculate the electronic and structural properties of the TMDs monolayers. The PBE GGA (Medvedev et al., 2017) approximations of the exchange-correlation functional and pseudopotentials (PAW) were applied. The necessary input data i.e., atomic positions, lattice constant, and symmetry must be defined for the structural properties of the TMDs. Before running the electronic calculations, it is essential to find out the best structural properties for the studied materials so that the relaxed lattice values give minimum total energy for the ground state. If experimental values of the lattice constant are used without relaxation, then the final energy will not be minimized because the material will be under stress, which will affect its electronic properties. Also finding inter layer distance for a monolayer of TMDs is very crucial. Before relaxation calculation for lattice constant and atomic positions, the two important convergence tests were performed. One is related to kinetic energy cut -off and the other is concerned with k-points.

2.6 Electronic and Magnetic Properties of Mono Layer of MoSe₂ and WSe₂

To calculate the electronic and magnetic properties of mono layer $MoSe_2$ and WSe_2, they are subjected to different methods for bandgap tuning. Vacancy creation and doping are used in this research. Electronic band graphs and DOS are plotted and analysed further to get the bandgap values, formation energies, and magnetic moments.

2.6.1 Monolayer TMD's Band Diagram and Khon-Sham Bandgaps

To obtain band diagram and bandgaps, a set of computations is needed to be run on VASP which later needs to be analysed. Band diagram of monolayer $MoSe_2$, WSe_2 primitive cell using GGA approximation has been calculated. Also, the bandgap has been calculated for the two TMDs. Bandgaps are formulated along with the high symmetry points in the Brillouin zone by using the Γ-M-K-Γ path. The electronic band structure of $MoSe_2$ and WSe_2 were calculated, and it was evident that both (Ahmed et al., 2020) monolayers have a direct bandgap.

2.6.2 Projected Density of States (PDOS) of Monolayer TMDs

In the next chapter of results, the Density of State (DOS) of WSe_2 and $MoSe_2$ will be discussed in detail. The DOS was found by using GGA approximation of the exchange–correlational functional and the pseudo potential for the monolayer primitive cell. DOS of each atom was calculated and then summed up as total DOS as a linear combination of each atomic orbital. Two methods were employed for bandgap tuning, these are:

   i.   Creating vacancies (structural defects).

   ii.   By substitutional doping.

Bandgaps and DOS are calculated after applying two tuning methods. The geometrical structure and electronic properties were calculated by using DFT of doped and

undoped MoSe$_2$ and WSe$_2$ using VASP.PBE function of GGA was used for the electron-ion interactions and exchange-correlational potential respectively (Hamann et al., 1979; Perdew et al., 1996). The super cell is 6x6x1 having 36 Mo and W atoms (light pink),72 Se (green ball) and 1 Ru (blue) and Rh atom(red). The high energy cut off for the plane wave is set at 400 eV and the Brillion sample is 5x5x1 by k sampling grid. The structure is relaxed and the binding energy (E$_b$) of the doped system is calculated to assess the stability of doped WSe$_2$ and MoSe$_2$.

$$E_b = E_{vacancy} + \mu_M - E_{doped}$$
(Equation 2.17)

Where V$_{acancy}$ is the total energy of the Monolayer with one Se vacancy and μ$_M$ is the chemical potential of the dopant. If E$_b$ is positive, it means that it is favourable to be found at the site of Se. The bandgap is reduced significantly by doping hence supplying a good mechanism for bandgap tuning.

2.6.3 Substitutional Doping

It has been studied widely by DFT that substitutional doping involving bandgap tuning affects the electronic properties of the material (Santhosh et al., 2020). Graphene has no direct band and hence it does not show a semiconductor property and hence cannot be used as a semiconductor. Substitutional doping is a way to open the bandgap of Graphene (Lee et al., 2018). Various researchers have reported the magnetic behaviour of MoSe$_2$, and WSe$_2$ after vacancy defect and substitutional doping (Mabelet al., 2020; Yang et al., 2019). Here in this research two metals Rh and Ru will be studied for their impact on the two monolayers. The electronic and magnetic properties of the doped semiconductor will be analysed. Hence substitutional doping and vacancy defects affect the electric, electronic, and even optical properties (Deng et al., 2018; Yang et al., 2019) of the TMD.

Here we systematically studied the structural, electronic, and magnetic properties of the two mentioned TMDs (MX_2; M=W, Mo; X=Se) monolayers with atomic sized structural defects. We considered the vacancy defects including mono (1V), tri (3V) and Penta (5V) vacancies as well as the substitutional doping of TM Ru and Rh. They are chosen as dopants in $MoSe_2$ and WSe_2 monolayers. Ruthenium, Ru is a transition metal of group 8 in the periodic table, belonging to the Platinum Group with atomic number 44. Ru has only one electron in the outermost shell. It is a white polyvalent metal. Rhodium on the other hand is a silvery-white chemical element of atomic number 45 which is a rare, hard, and chemically inert transition metal. It belongs to group 9 of the periodic table and is face centred cubic (*fcc*) in structure.

These defects change the electronic and magnetic properties of the monolayers. These structural defects and substitutional doping results in semiconductor to metal transition. Later, the total magnetic moment is also calculated and tabulated in the results.

2.7 Computational Methods

The calculation was made using Vienna Ab-Initio Simulation Package (VASP). The exchange correlations functional are represented by Projected Augmented Wave (PAW) pseudopotentials and Perdew-Burke-Research of functional of the GGA approximation (Hamann et al., 1979; Perdew et al., 1996). The configuration used for supercell is 6x6x1 which holds 36 W, Mo atoms and 72 Se atoms. When Metals Rh and Ru enter the lattice of the semiconductors, we will consider substituting Se atoms with them by creating vacancy defects first. A huge cut of the energy of 400 eV is set. A 5x5x1 k-point sampling grid is used. Structures are relaxed until a force and energy are less than 10^{-3} eV/A˚ and $1.0x\ 10^{-5}$ eV/atom. To avoid reciprocity amongst periodic

slabs, layers vacuum of 20 A˚ was created. Further, formation energy was calculated E_f by using the following equation.

$$E_f = E_{doped} - E_{undoped} + \mu_{Se} - \mu_M \qquad \text{(Equation 2.18)}$$

where E $_{doped,}$ and E $_{undoped}$ are the total energies of monolayer WSe_2 and $MoSe_2$ with and without dopant atoms. μ_M is the chemical potential of the doped elements? In this Chapter, the bandgap tuning methods used in the research were discussed in detail. The theoretical background was also supplied for the research design.

Chapter 3: Results

3.1 Background

In the recent past, 2D layered materials have gained a lot of attention for researchers in material science. Due to their typical structure, they exhibit different characteristics than their bulk counterparts (Novoselov & Geim, 2007; Neto et al., 2009; Novoselov et al., 2005; Zhang, 2016). With booming interest in Graphene synthesis, it was a starting point in further exploration of 2D materials (Novoselov et al., 2004). Since Graphene does not have a direct bandgap hence it cannot be used in many nano technological devices. Some of the 2D TMDs are very useful because of having a direct bandgap optical transparency and mechanical strength (Dıez-Pérez et al., 2015; Kuc et al., 2015; Zeng et al., 2012).

Many researchers have contributed to the study of the 2D monolayer of TMD which is used for bandgap tunning as they offer a direct bandgap as compared to Graphene.$MoSe_2$ and WSe_2 are such two promising compounds which are great in terms of photo voltaic devices and other nano technological applications. Recently (Zhao et al., 2017) made a remarkable contribution by studying the effects of nonmetals doping into $MoSe_2$ for photocatalytic purposes. They found out that nonmetals such as (H, B, C, Si, N, P, As, and the like) are energetically favoured to Se vacancies except for B and C doped. Furthermore, they also discovered that an even number of valance electrons when doped with $MoSe_2$ results in *p*-type conductivity while the odd number of electrons when doped with $MoSe_2$ can have *p*-type or *n*-type conductivity and they have better photocatalytic properties.

Another recent work (Tian et al., 2020) investigated the metal-doped (Fe, Mn, Co, Ni) $MoSe_2$ by DFT. Their work suggests that there were insignificant changes in the crystal

structure after the incorporation of these metals, but formation energies show a Se rich structure is more likely to be stable than Mo rich conditions. They also saw a semimetal behaviour when doped with Fe and (Mn, Ni) as well as magnetic properties were calculated. Another research (Urbanová et al., 2021) indicated the effects of Re doping in TMDs and concluded that it enhances the photoelectron chemical properties of the doped $MoSe_2$ and WSe_2. They also saw an increase in photocurrent response in doped WSe_2 and $MoSe_2$ upon exposure to UV light.

The researchers (Jain et al., 2020) investigated Hydrogen Evolution Reaction (HER) in doped $MoSe_2$. They used DFT to study the relationship between TM (Fe, Ni, Mn, Co) doping and Se vacancies in $MoSe_2$ and analysed the Hydrogen Evolution Reaction (HER phenomenon). They concluded that electron-rich TM dopants change the $MoSe_2$ electronic structure towards HER basal planes and Se vacancies support the HER.

3.2 Bandgap Tuning of the $MoSe_2$ Monolayer Through Vacancy

In this section, the bandgap tuning of $MoSe_2$ through vacancy will be discussed. The next sections explain the two processes and results taken by creating defects (vacancies).

3.2.1 Pristine $MoSe_2$ Monolayer

To understand the effects of bandgap tuning, we need to discuss the structural and electronic properties of the pristine $MoSe_2$ monolayer first.
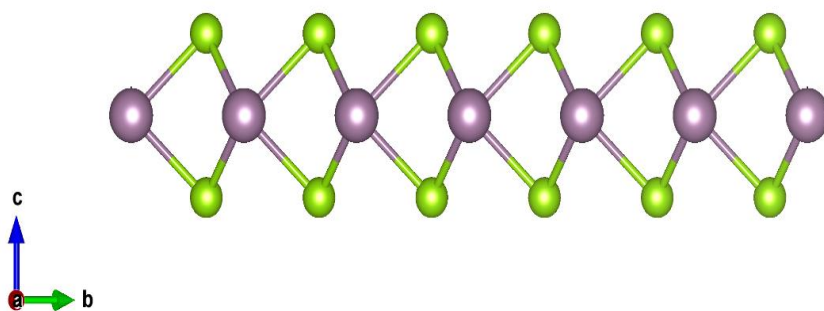
Figure 2: Side view of the 6 x 6 x 1 Supercell of the Pristine 2D MoSe$_2$ Material
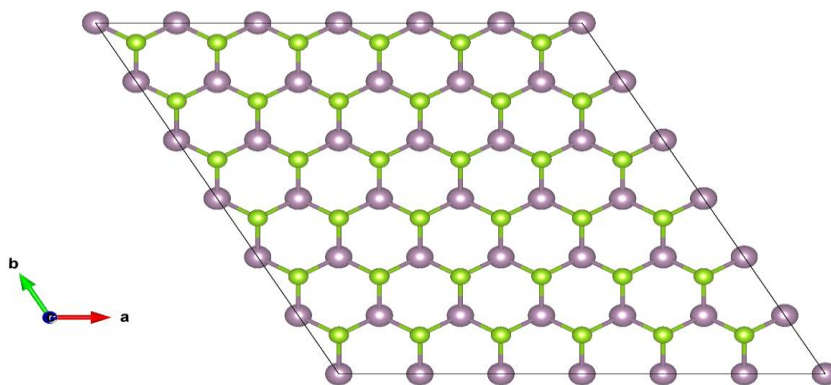
Figure 3: Top view of the 6 x 6 x 1 supercell of the Pristine 2D MoSe$_2$ Sheet

As shown in Figures 2 and 3, the 2D TMD MoSe$_2$ is similar in structure to graphene as it constitutes of Se-Mo-Se hexagonal planes which are covalently bonded. Weak Vander Waal forces are keeping the crystal intact. Previous research work has shown that the hexagonal structure is the most stable configuration for MoSe$_2$ (Ataca et al., 2012). Electrons are confined to 2D, and the M-X covalent bond is made due to *p-d* orbitals. Both MoSe$_2$ and WSe$_2$ have hexagonal crystal structures with Mo and W centred at the trigonal coordination with the six nearest Se atoms. The 6x6x1 super cell was created for bandgap tuning as shown in Figure 3 by creating Vacancies in the super Cell.

3.2.2 Electronic Properties of the Pristine MoSe₂ Monolayer

To understand the effect of vacancies in TMD $MoSe_2$, first, the calculations were done on the monolayers of the compound in the pure form band structure of $MoSe_2$ as seen in Figure 4 which shows high symmetry directions in the first Brillouin zone. It is also complemented by looking at the band structures of the compound. $MoSe_2$ shows a Semiconductor nature with no branches across the Fermi level. A direct bandgap existed at the maxima of the valence band and the minima of the conduction band were located at the same symmetry point M and it is consistent with the previous results (Medvedev et al., 2017). To study the electronic properties of the pristine $MoSe_2$, density of state (DOS) is evaluated and shown in Figure 5. The DOS plot shows a gap between Valance Band Maxima (VBM) and Conduction Band Minima (CBM) which explains $MoSe_2$ to be a semiconductor.
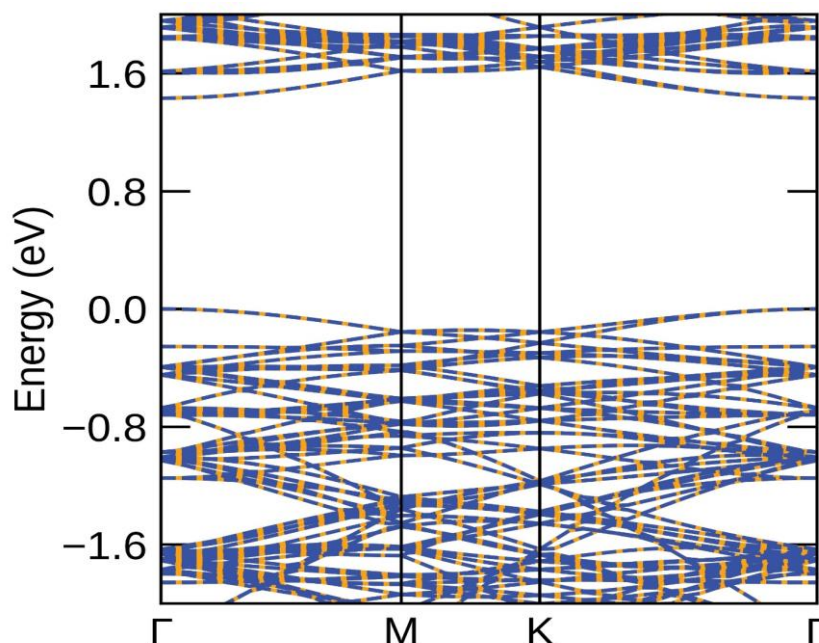
Figure 4: Band Structure of the 6 x 6 x 1 Supercell of the Pristine 2D MoSe₂ Sheet
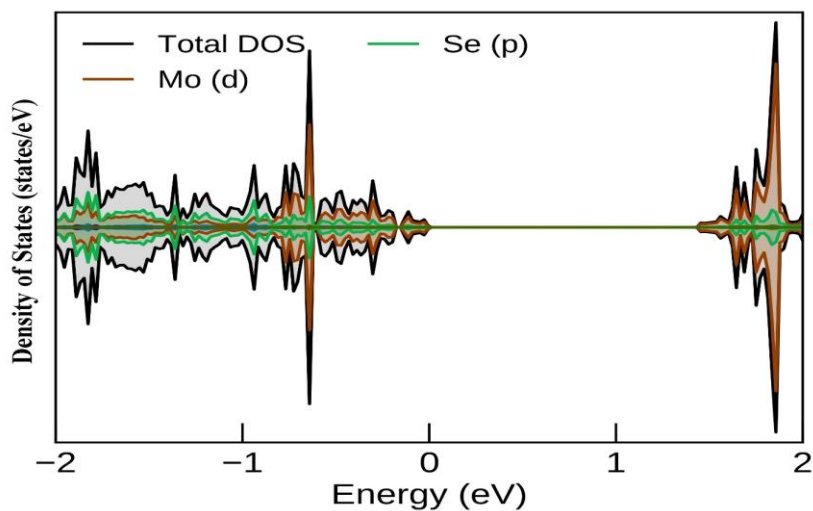
Figure 5: Density of States of the 6 x 6 x 1 Supercell of the Pristine 2D MoSe$_2$

It also displays that the bandgap between VBM and CBM occurs mainly due to the '*d*'
orbital of Mo and there is a small contribution by the p orbital of Se is also noticeable.
The bandgap of pristine MoSe$_2$ is found to be 1.432 eV which is consistent with the
previous experimental and theoretical data as indicated in Table 2.

Table 2: The Theoretical and Experimental Energy Band-Gaps of the Pristine MoSe$_2$

Structure	Method	Bandgap (eV)
MoSe$_2$	Experimental	1.59 [a]
MoSe$_2$	Experimental	1.55 [b]
MoSe$_2$	GGA	1.43 [c]
MoSe$_2$	GGA	1.432 [d]

a: (Island et al., 2016),
b: (Li et al., 2018),
c: Deng, Li, Li, & Nanostructures, 2018),
d: This work.

3.2.3 Electronic and Magnetic Properties of MoSe$_2$ with Vacancies

To calculate the Electronic and magnetic properties of MoSe$_2$, random vacancies are created at Mo sites and band structure and DOS are plotted. In this research, mono tri and Penta vacancies are created to find the effects on MoSe$_2$. The structure of MoSe$_2$ with the mono vacancy is presented in Figure 6. Figure 6 shows the mono vacancy of the Mo atom which significantly reduces the bandgap to 0.89 eV.

Figure 7 illustrates the DOS of MoSe$_2$ with a single vacancy. It shows that the bandgap has reduced. The bandgap reduction is also clear from the band structure in Figure 8.
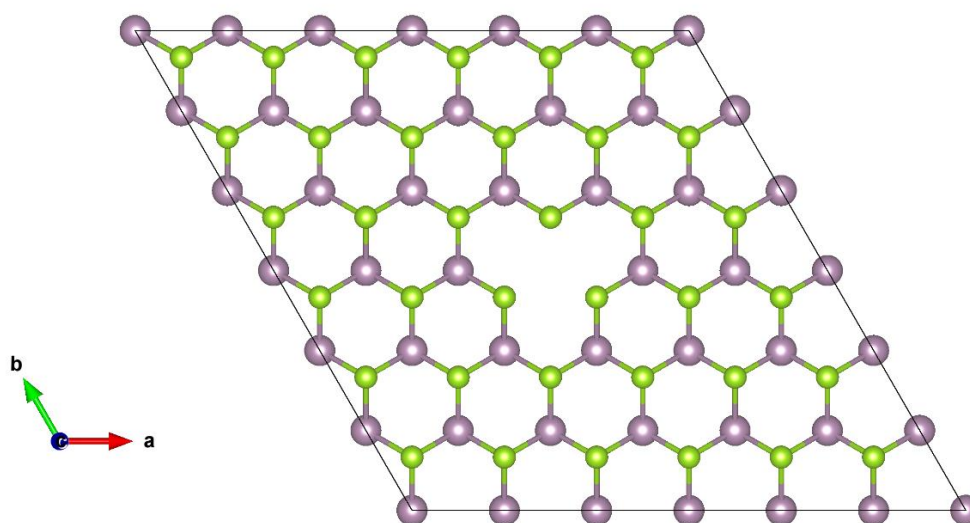
Figure 6: Top View of the 6 x 6 x 1 Supercell of the Defected 2D MoSe$_2$ Sheet with a Mono Vacancy (1 V) In the Middle
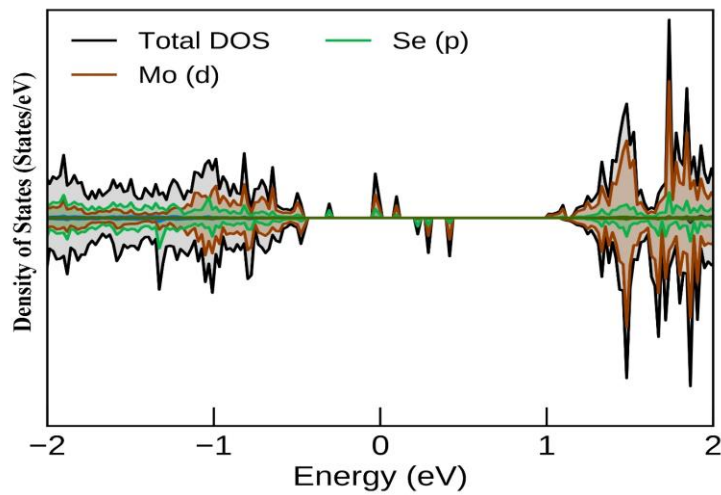
Figure 7: Density of States of the 6 x 6 x 1 Supercell of the Defected 2D MoSe$_2$
Sheet with a Mono Vacancy (1 V)
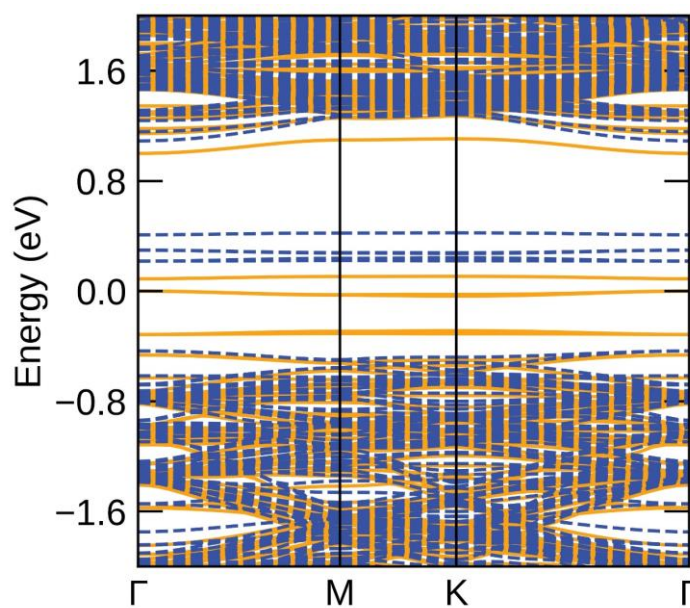
Figure 8: Band Structure of the 6 x 6 x 1 Supercell of the Defected 2D MoSe$_2$ Sheet
with a Mono Vacancy (1 V)

Figure 9: Top View of the 6 x 6 x 1 Supercell of the Defected 2D MoSe$_2$ Material with Three Vacancies (3 V)

Figure 10: Total and Partial Density of States of the 6 x 6 x 1 Supercell of the Defected 2D MoSe$_2$ Sheet with Three Vacancies (3 V)

Figure 11: Band Structure of the 6 x 6 x 1 Supercell of the Defected 2D MoSe$_2$ Sheet with Three Vacancies (3 V)

Figure 12: Top View of the 6 x 6 x 1 Supercell of the Defected 2D MoSe$_2$ Material with Five Vacancies (5 V)
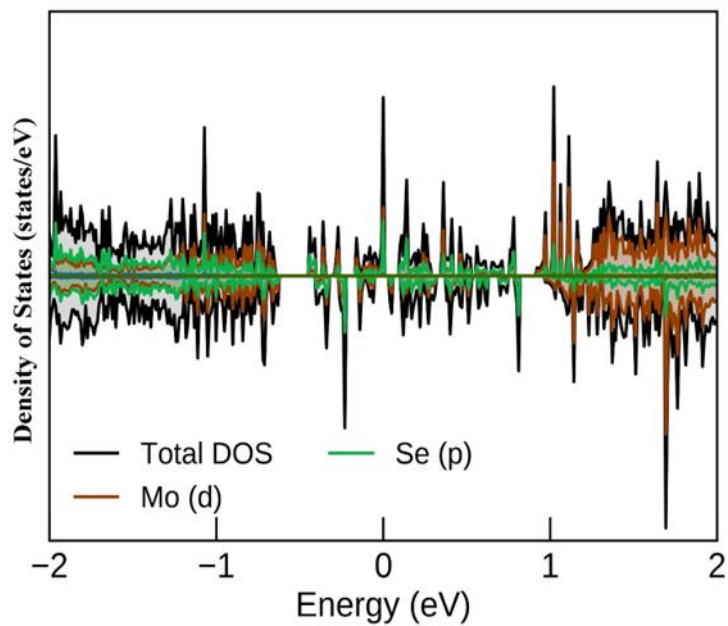
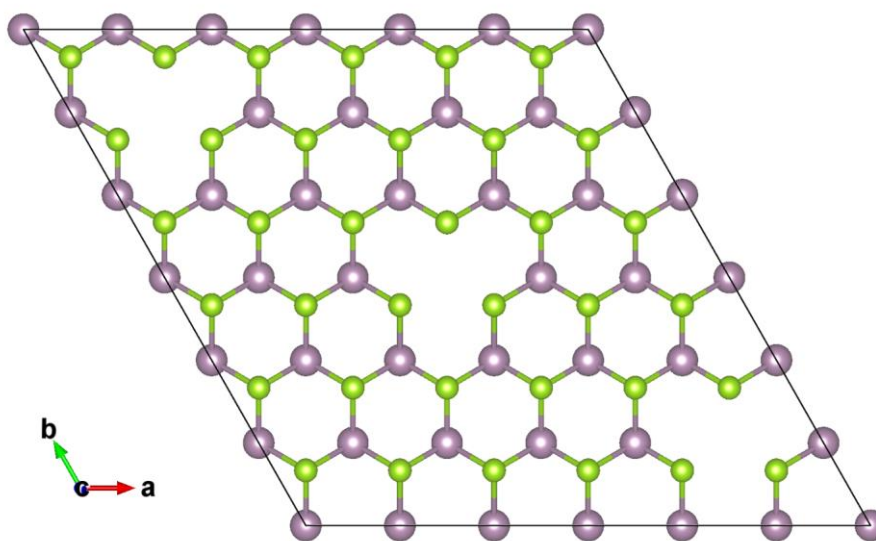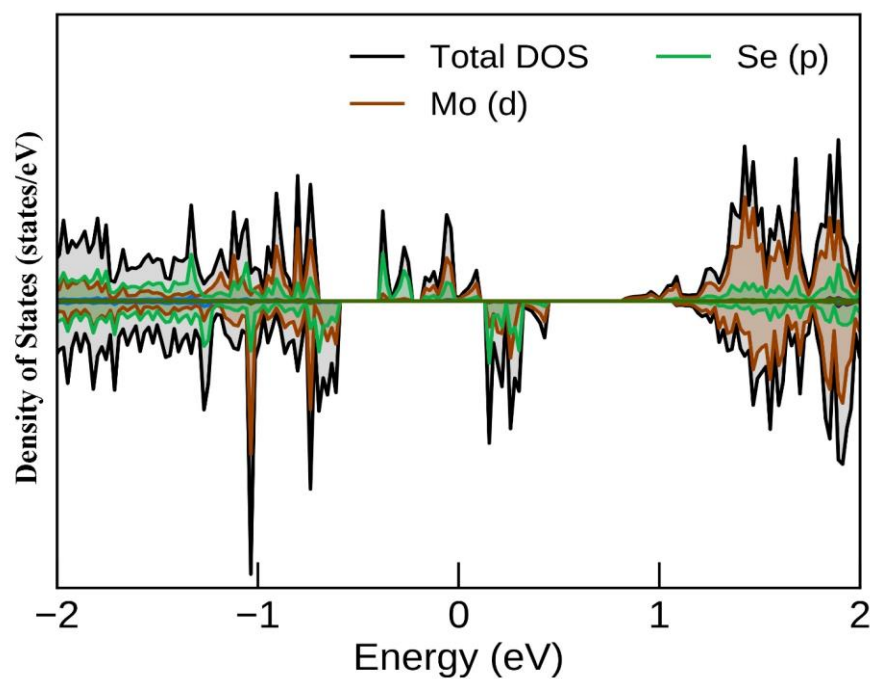Figure 13: Total and Partial Density of States of the 6 x 6 x 1 Supercell of the Defected 2D MoSe₂ Material with Five Vacancies (5 V)
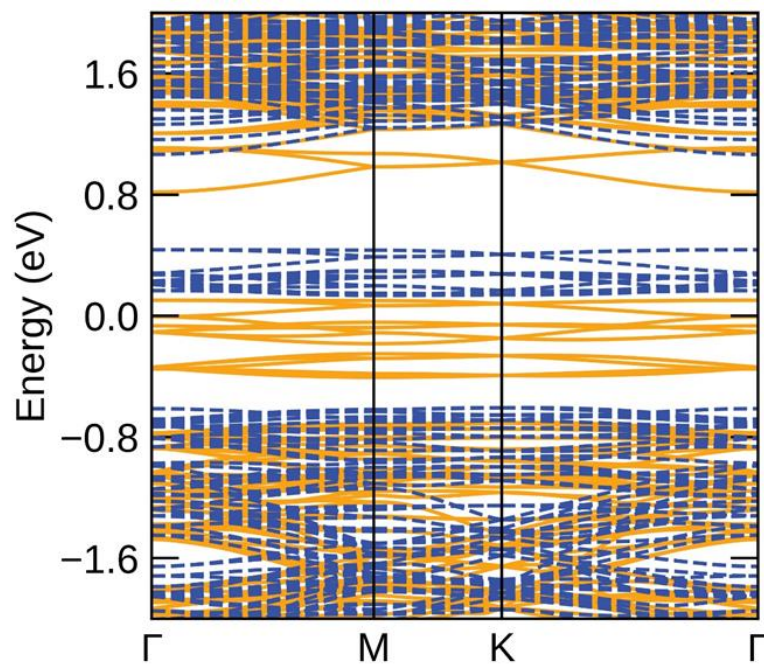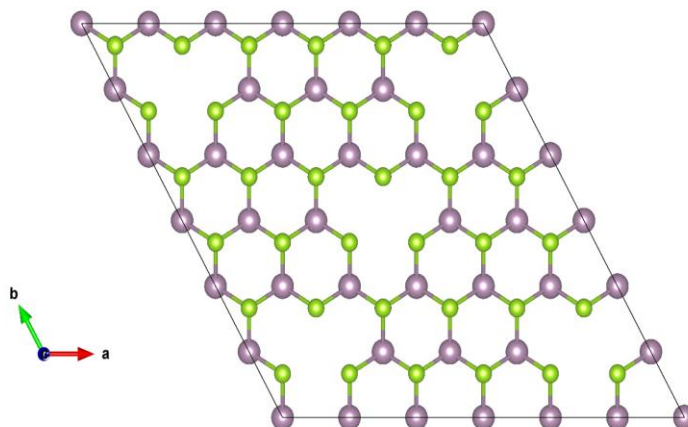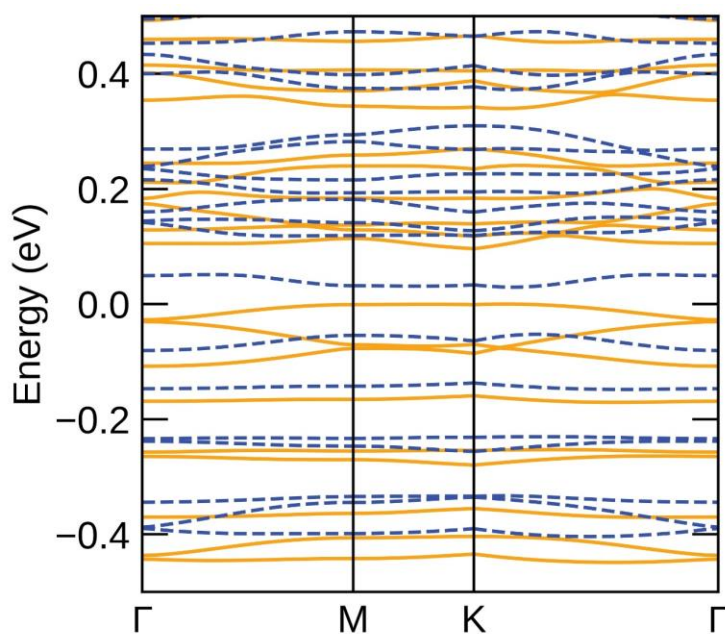

Figure 14: Band Structure of the 6 x 6 x 1 Supercell of the Defected 2D MoSe₂ Sheet with Five Vacancies (5 V)

Table 3: Summary of the Effect of Vacancy Defects in MoSe$_2$ Monolayer

System	Formation Energy (eV)	Band Transition	Conductivity	Bandgap (eV)
MoSe$_2$	-0.725	Γ---- Γ	Semiconductor	1.432
V 1-MoSe$_2$	5.781	Γ---- Γ	Semiconductor	0.089
V 3-MoSe$_2$	17.244	-----	Metal	-----
V 5-MoSe$_2$	22.758	K----Γ	Semiconductor	0.029
MoSe$_2$	-0.725	Γ---- Γ	Semiconductor	1.432

Figure 9 shows the top view of MoSe$_2$ with tri vacancies and Figure 10 illustrates the DOS of the defected structure. We can see that though the band structure, and bandgap have reduced further, the structure illustrates a metallic character. Figure 11 shows the spin-polarized band structure of MoSe$_2$ with tri vacancies. The yellow solid line shows the spin-up channel while the blue dashed line is the spin-down channel. In the spin-up channel, the electrons cross the Fermi level while in the spin-down channel, there is a semiconducting bandgap is present. A material which has a bandgap in one spin channel while it is semiconducting in the opposite channel behaves as a half-metallic material. So, the MoSe$_2$ with tri vacancy behave as a half-metal which is visible in the DOS plot in Figure 11.

Figure 12 shows the top view of the 6x6x1 supercell of the defected 2D MoSe$_2$ with five vacancies. Further vacancy creation (five vacancies) within the MoSe$_2$ monolayer makes it metallic as shown in the DOS and band structure plots presented in Figure 13 and Figure 14. As summarized in Table 3, we see that the bandgap reduces as the number of vacancies increases. Tri vacancies induce metallic character in MoSe$_2$. Table 4 summarizes the magnetic moments calculated. All the created vacancies,

induce the magnetic moments. All the created vacancies, induce the magnetic moments. To find the stability of $MoSe_2$ monolayer with vacancies, formation energy is calculated and listed in Table 5. It shows the calculation for the formation energy with vacancies in $MoSe_2$. It is evident from Table 5 that a lower number of vacancies are thermodynamically stable.

Table 4: Summary of the Magnetic Moments of all the $MoSe_2$ DFT Studied Material with Vacancy Calculated by the DFT-GGA Method

Structure	Method	Magnetic Moment (μ_B)
$MoSe_2$ (1 V)	GGA	3.99
$MoSe_2$ (3 V)	GGA	12.000
$MoSe_2$ (5 V)	GGA	2.00

Table 5: Formation Energy of the $MoSe_2$ Monolayer with Vacancies

Number of Vacancies	1V	3V	5V
E_{form} (eV/f.u.c)	5.781	17.244	22.758

3.3 Bandgap Tuning of the $MoSe_2$ Through Substitutional Doping

Monolayer $MoSe_2$ has a hexagonal crystal structure where Mo exists at the trigonal prismatic with six nearby Se atoms. A supercell of 6x6x1 dimension was created as shown in Figure 2 in which one Mo atom was replaced with one Rh atom with a doping concentration of 2.7%, 8.3% and 13.88% respectively. The geometrical structure was relaxed and optimized before doping with TM atoms. The closing value of the ion radius of Mo with the TM dopants Rh and Ru suggest that there will not be minimum distortion in the structure of doped TMD $MoSe_2$.

3.3.1 Effects of Rh Doping on the Electronic and Magnetic Properties of the MoSe₂ Monolayer

The band structure results of the MoSe₂ monolayer with 2.7%, 8.3% and 13.8% concentrations of Rh doping are presented in Figures 15-17 and Figure 19. The Fermi level shifts to the high energy region in all the doped MoSe₂. It happens as the $3d$ electron of Rh dopant replace with that of Mo in the host MoSe₂ supercell. A flat impurity band can be seen by adding the impurity metal Rh which enhances the electronic transport property. Furthermore, all the band structures are asymmetric between the spin-up and spin-down channels which suggests that 3d TM dopants can induce spin-polarized states.

The results are consistent with the magnetic moment calculated in Table 6. It shows a semiconducting behaviour with a bandgap of 0.568 eV, and 0.022 eV by 2.7% and 13.88% concentration of Rh metals, respectively. However, for an 8.3% concentration of Rh, as shown in Figure 17, many spin up branches cross the Fermi level and yield metallicity, while the spin-down band structures stay semiconducting with a bandgap of 0.431 eV showing half-metal feature which can be used for spin filter device applications.

The Magnetic moments are calculated and listed in Table 6. The total magnetic moment is greatest in the case of 8.3% doped Rh TM which results in half-metallic character and reduces to 1.002 μ_B for highly Rh doped (13.88%) MoSe₂. Figures 16-18 and Figure 20 depict the corresponding DOS of Rh doped in high, low, and moderate concentrations, respectively. Fermi levels move from the valence band maximum to the higher energy regions. The asymmetric distribution of DOS is clear between spin up and spin down states confirming the formation of magnetic moments.
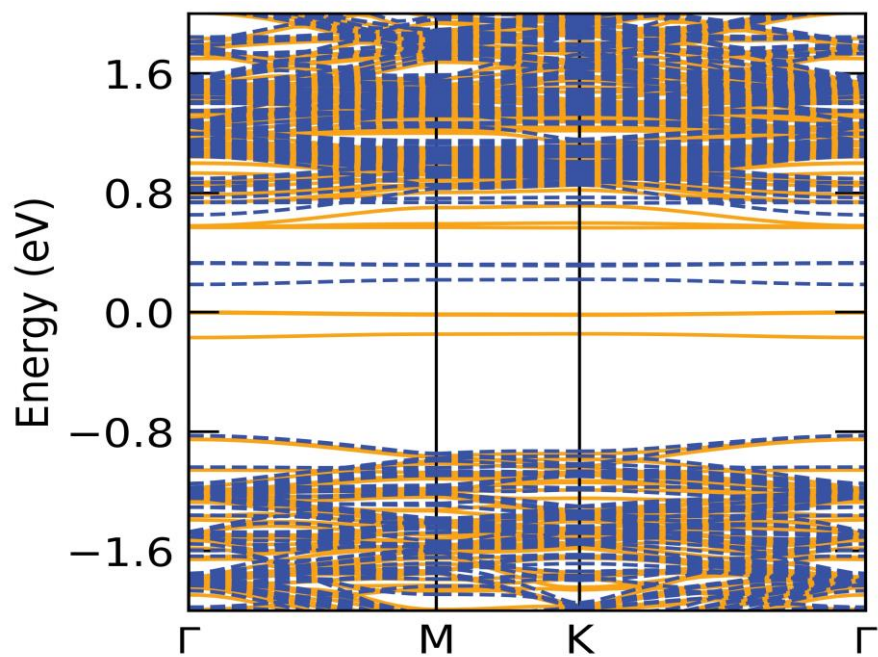
Figure 15: Band Structure of the MoSe₂ with 2.7% Concentration of Rh Atom
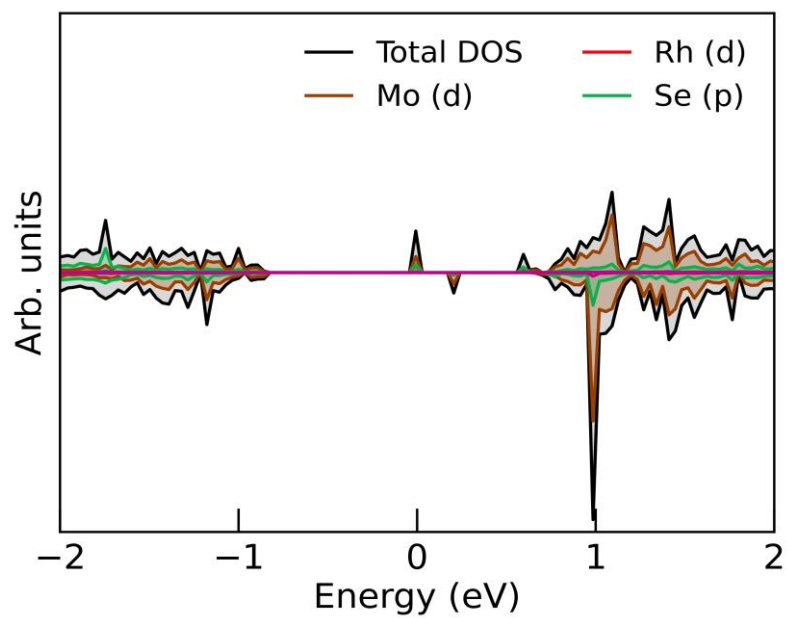
Figure 16: DOS of the 2.7% Rh Doped MoSe₂
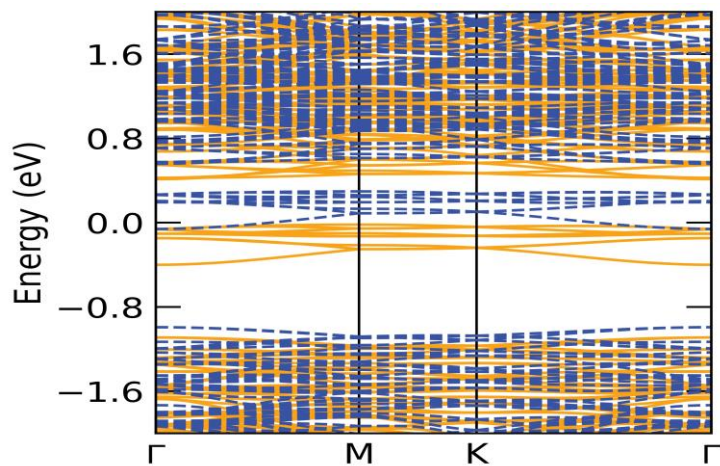
Figure 17: Band Structure of the MoSe₂ with 8.3% Concentration of Rh Atom
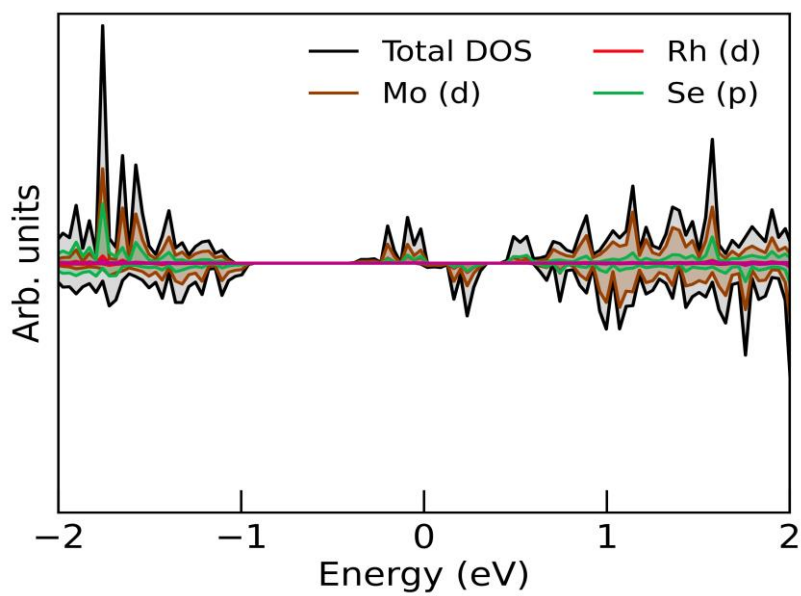
Figure 18: DOS of the 8.3% Rh Doped MoSe₂
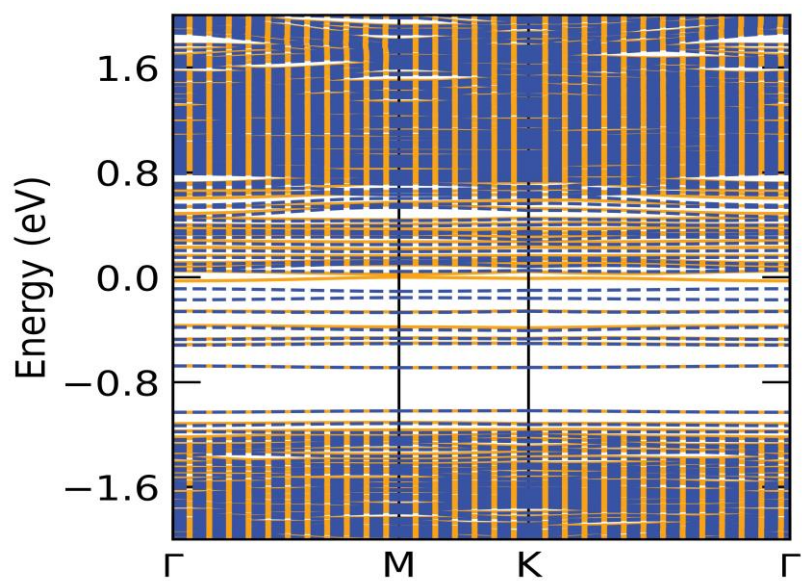
Figure 19: Band Structure of the MoSe₂ with 13.88% Concentration of Rh Atom
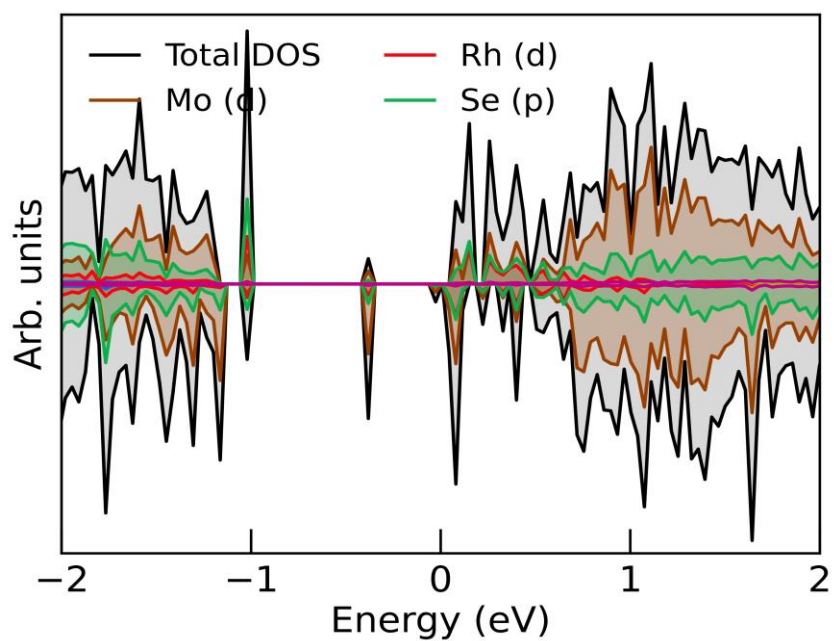
Figure 20: DOS of the 13.88% Rh Doped MoSe₂

Table 6 summarizes the effect of TM doping of Rh metal on the monolayer $MoSe_2$. The bandgap significantly reduced from 1.432 to 0.022 eV as the concentration of Rh dopant increased from 2.7% to 13.88%. This confirms the fact that as the doping concentration of Group IV metal Rh increases, the bandgap reduces to an appreciable value making $MoSe_2$ a favourable candidate for bandgap applications. The above results also reveal the fact that Monolayer $MoSe_2$ changes its character from a semiconductor to a half-metallic one as the doping concentration increases from Low (2.7%) to Medium (8.3%). The transition is clear at M and Γ points in Figure 3.20. It regains its character of semiconductor TM again by heavy concentration i.e., 13.88% of Rh doping. The transition happens at the Γ points.

Table 6: Summary of the Effects of Rh Doping on $MoSe_2$ Monolayer

System	Formation Energy (eV/f.u.c)	Band Transition	Conductivity	Bandgap (eV)	Magnetic Moment
$MoSe_2$	-0.725	Γ---- Γ	Semiconductor	1.432	----
$MoSe_2$ (2.73% Rh)	-1.721	Γ----Γ	Semiconductor	0.568	2.9799
$MoSe_2$ (8.3% Rh)	4.527	M ---Γ	Semi-metallic	0.431 Spin-up	8.9235
$MoSe_2$ (13.88% Rh)	9.050	Γ----Γ	Semiconductor	0.022	1.002

3.3.2 Effects of Ru Doping on the Electronic and Magnetic Properties of the MoSe$_2$ Monolayer

In this section, the effects of Ru doping in MoSe$_2$ are presented. Various concentrations of Ru are used, and the electronic and magnetic properties are calculated. The concentrations are 2.7%, 8.3% and 13.88% respectively. The band structure and DOS are plotted to analyse various characteristics of Ru doped MoSe$_2$. The properties calculated are bandgap values, formation energies magnetic moment, conductivities, and transition points.

Figures 22-24, and Figure 26 show the DOS of doped MoSe$_2$ with 2.7%, 8.3% and 13.8% concentrations of Ru, respectively. With a 2.7% (low) concentration MoSe$_2$ demonstrates a half-metallic character as shown in Figure 21 of band structure, where the Fermi level crosses the spin-up channel, and the spin-down channel is a semiconductor. Medium (8.3%) and high (13.8%) of Ru says a semiconductor behaviour as shown by DOS in Figure 22 and Figure 24. The band structure in Figure 23 and Figure 25 show the same semiconductor behaviour.

Other interesting findings listed in Table 7 are the values of the bandgap energies. Doping of Ru TM into MoSe$_2$ resulted in lowering the bandgaps from 1.432 eV to 0.271 eV which is 81% less and more significant. The bandgap values for the Low (2.7%) medium (8.3%) and high (13.8%) concentration were calculated as 1.198 eV, 0.379 eV and 0.271 eV, respectively.
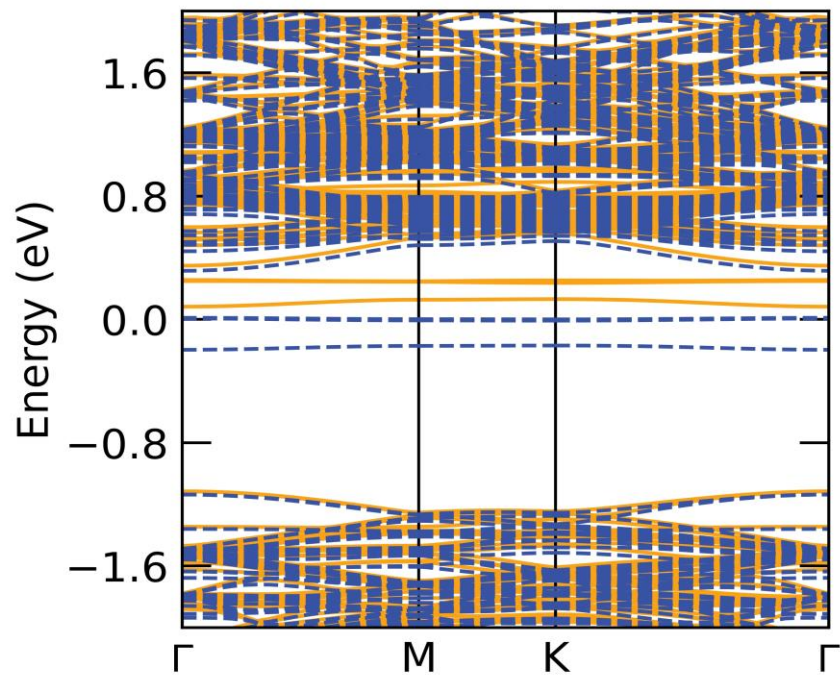
Figure 21: Band Structure of the 2.7% Ru Doped MoSe$_2$
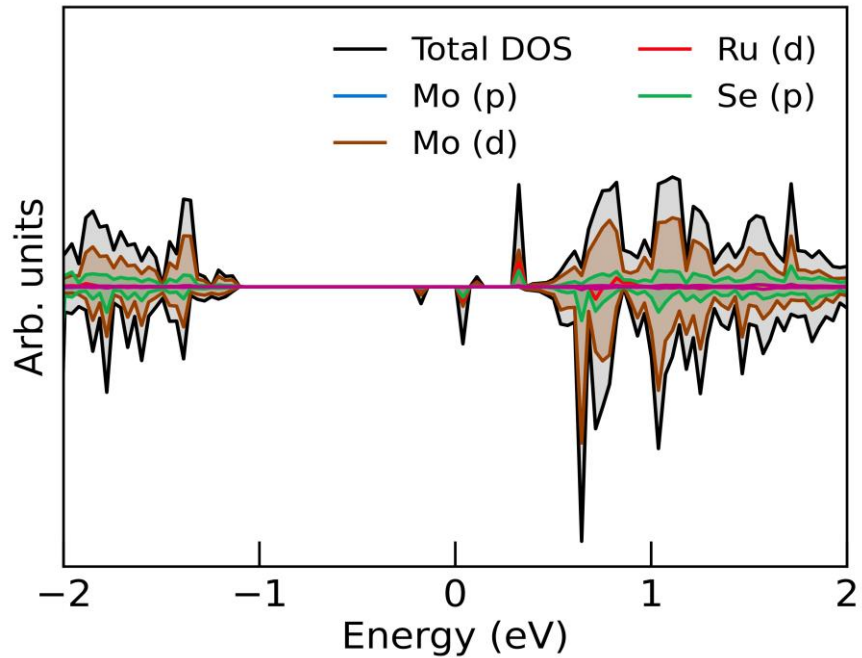
Figure 22: DOS of 2.7% Ru Doped MoSe$_2$
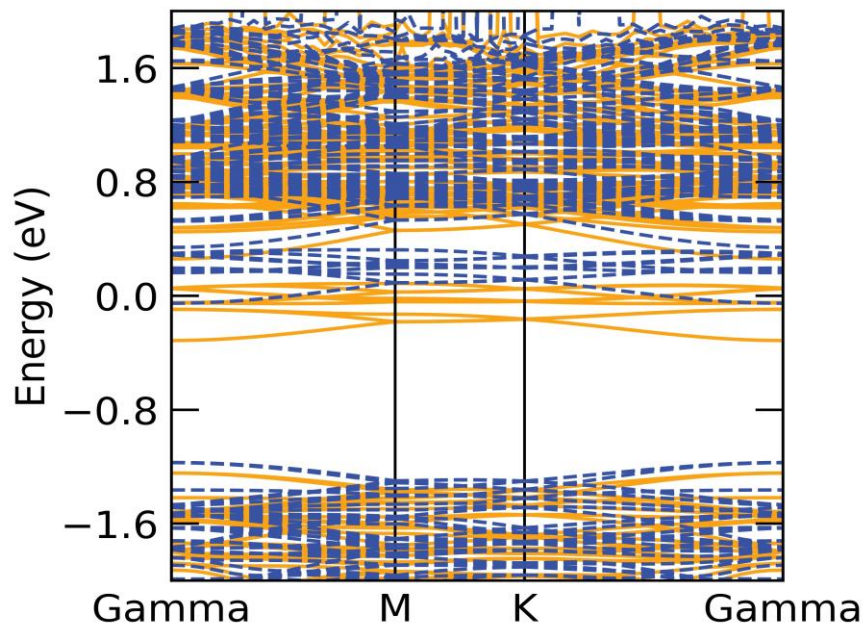
Figure 23: Band Structure of the 8.3% Ru Doped MoSe$_2$
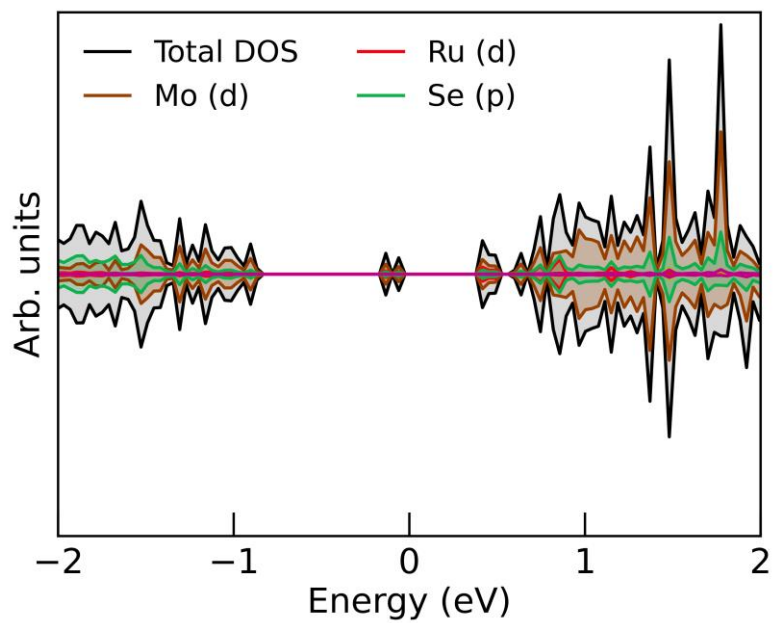
Figure 24: DOS of 8.3% Ru Doped MoSe$_2$
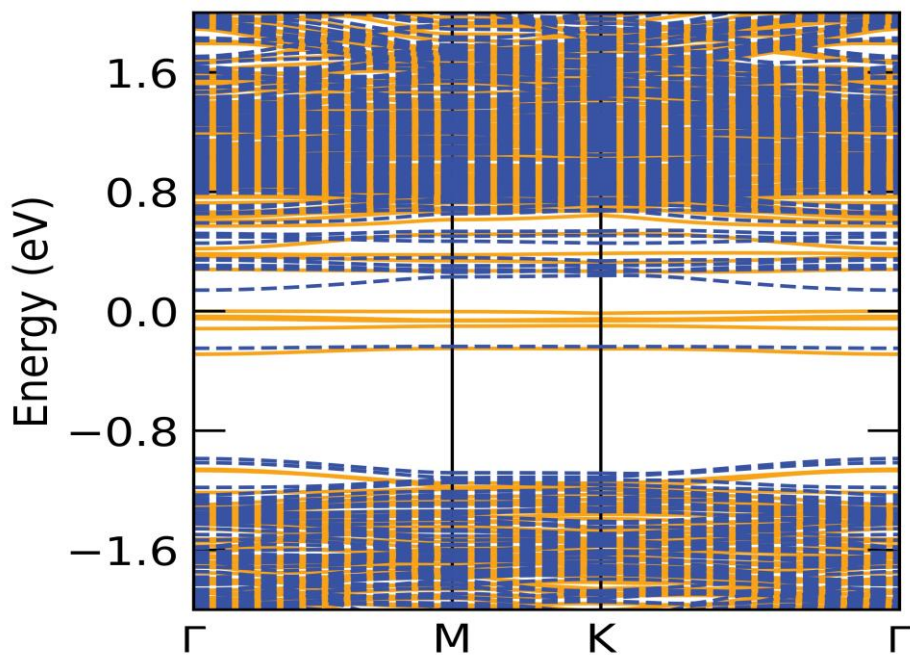
Figure 25: Band Structure of the 13.88% Ru Doped MoSe$_2$
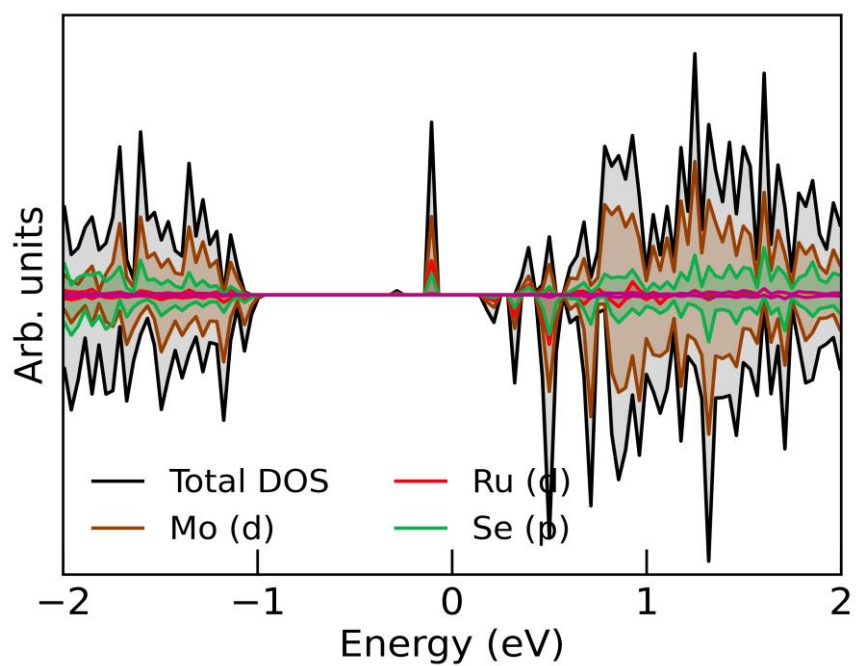
Figure 26: DOS of 13.88% Ru Doped MoSe$_2$

Formation energies were also computed and are listed in Table 7 below. It shows that a low concentration of Ru into $MoSe_2$ results in smaller formation energy of -2.367 eV making it a thermodynamically favourable configuration than the higher concentrations. Magnetic moments are also listed in Table 7 showing 2.00 μ_B, 5.365 μ_B, 4.533 μ_B for (2.7%), (8.3%) and (13.8%) concentrations of Ru dopant. The high (13.8%) and low (2.7%) concentration of Ru reveals the semiconductor nature of $MoSe_2$ as shown in Figure 25 and Figure 23 from the band structure results.

Whereas the Medium concentration (8.3%) of Ru metal in the monolayer of $MoSe_2$ gives a half-metallic nature since the Fermi level crosses the spin-up channel while the spin-down channel is a semiconductor as clear in Figure 24. More analysis of DOS shows that TM 3d orbitals play a key role near the Fermi Level, suggesting the magnetic properties induced by Ru impurities. Also, the 3d Mo orbitals find in the same energy ranges as Se 4p orbitals, suggesting strong hybridization interactions amongst them resulting in covalent bonds.

Table 7: Summary of the Effects of Ru Doping in $MoSe_2$ Monolayer

System	Formation Energy (eV/f.u.c)	Band Transitions	Conductivity	Bandgap (eV)	Magnetic Moment (μ_B)
$MoSe_2$	-0.725	Γ----Γ	Semiconductor	1.432	----
2.7% of Ru in $MoSe_2$	-2.367	Γ----Γ	Semi-metallic	1.198 spin-up	2.000
8.3% of Ru in $MoSe_2$	1.764	M---- Γ	Semiconductor	0.379	5.3658
13.88% of Ru in $MoSe_2$	6.931	Γ----Γ	Semiconductor	0.271	4.533

3.4 Bandgap Tuning of the WSe$_2$ Monolayer Through Vacancy

To understand the effect of vacancies and substitutional doping in TMD WSe$_2$, first, we have calculated the electronic properties of the pristine WSe$_2$. Many previous studies indicate that structural defects can impact the electronic, magnetic and mechanical properties of the materials (Song & Lü, 2018; Wu et al., 2019). Points defects and vacancy defects induce magnetism in graphene as reported by (Nair et al., 2012; Yazyev, 2010). Three different configurations for defects were studied in this research. All these defects 1 V, 3 V and 4 V indicate the 1, 3, and 4 vacancies created at the W site, resulting in point defects.

3.4.1 Pristine WSe$_2$ Monolayer

WSe$_2$ has been a subject of interest amongst the family of TMD because of its good electrical conductivity and strong photoluminescence properties and it is widely used in photocatalyst and photodetector applications.(Lin & Ni, 2016; Xin et al., 2017; Yang & Wu, 2016).WSe$_2$ is nonmagnetic which makes its use limited in spintronics (Seyler et al., 2019; Yang & Wu, 2016; Ye et al., 2019). Other research has suggested induced magnetic moments in WSe$_2$ by TMD's doping (Ahmed et al., 2020; Lin & Ni, 2016; Xin et al., 2017; You et al., 2018). It has been studied that NM dopant and vacancy defects can also bring magnetic moments in WSe$_2$ (Mabelet al., 2020; Yang et al., 2019). In this work, the effects of two metal dopants Rh and Ru on the electronic and magnetic properties of WSe$_2$ monolayers will be studied.
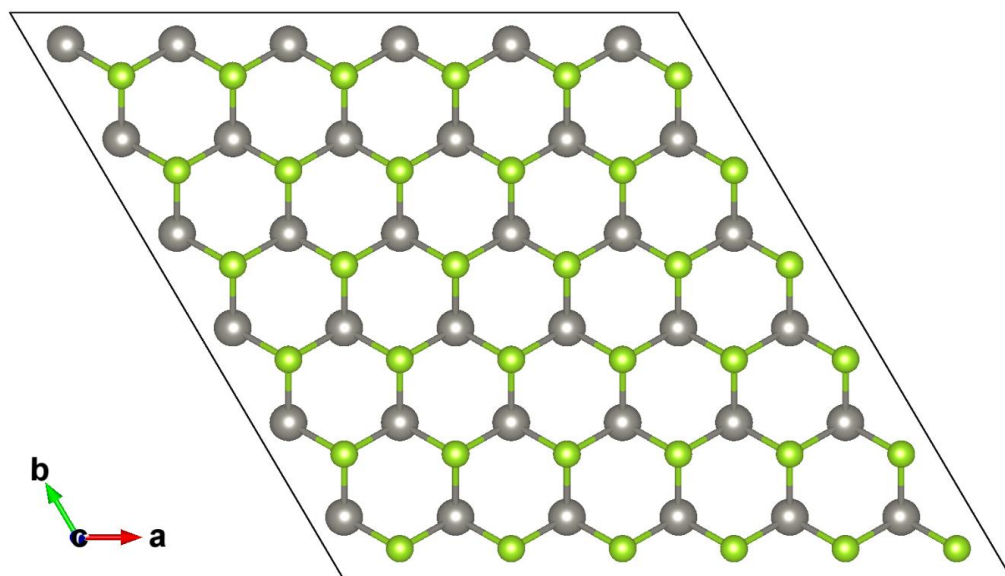
Figure 27: Side View of the 6 x 6 x 1 Supercell of the Pristine 2D MoSe$_2$ Material
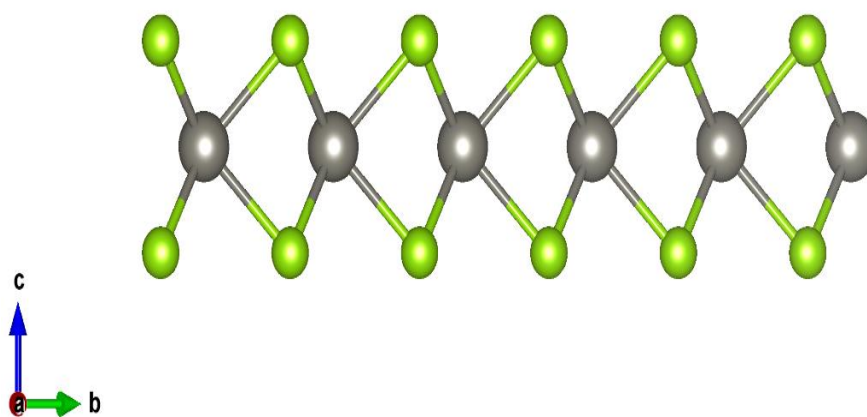
Figure 28: Top View of the 6 x 6 x 1 Supercell of the Pristine 2D WSe$_2$ Nanosheet
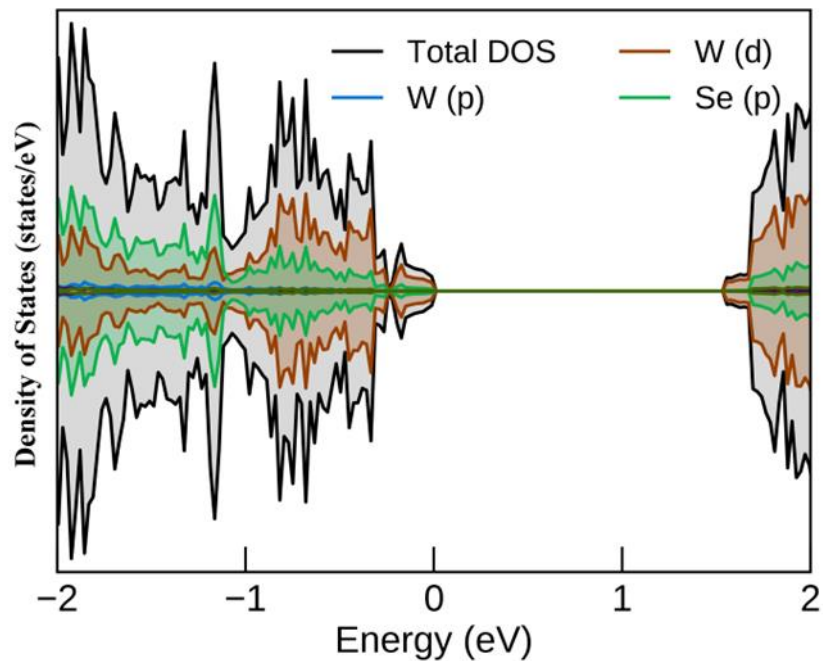
Figure 29: Total and Partial DOS of the 6 x 6 x 1 Supercell of the Pristine 2D WSe$_2$
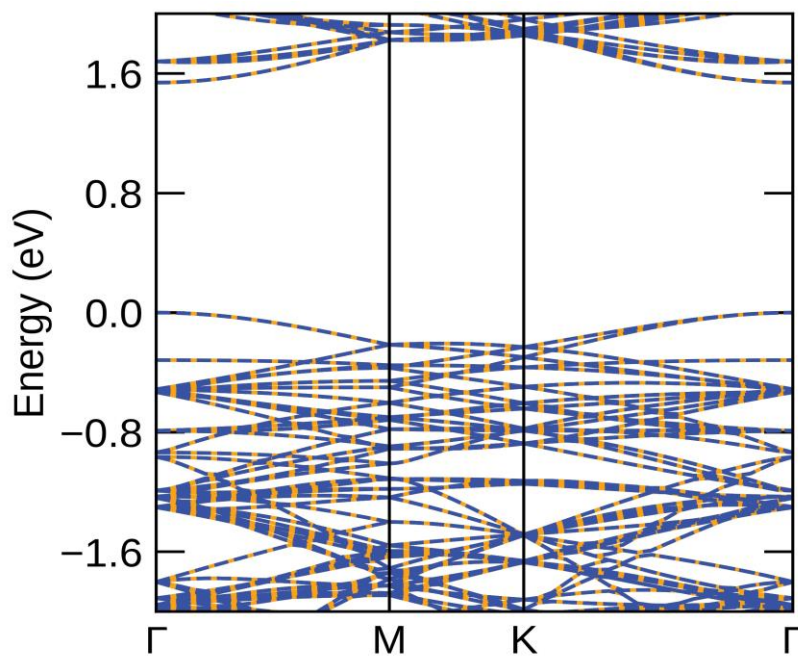
Figure 30: Band Structure of the 6 x 6 x 1 Supercell of the Pristine 2D WSe$_2$ Material

3.4.2 Electronic Properties of the Pristine WSe₂ Monolayer

WSe$_2$ is a semiconductor with a bandgap of nearly 1.6 eV (Ataca et al., 2012; Choi et al., 2017; Zhuang & Hennig, 2013). It's carrier mobility is 250 cm^2/V and the on-off ratio is higher than 10^6 at room temperature (Fang et al., 2012). All these interesting features make WSe$_2$ a very promising field of study.

Figures 29-30 show the DOS and band structure of the pristine WSe$_2$ monolayer. GGA approximation was used to find the bandgap of WSe$_2$ by DFT. The bandgap is found to be 1.539 eV at the Γ-points which is close to the experimental value of 1.73 eV. The next sections will show results for bandgap tuning of monolayer WSe$_2$ by creating vacancies and substitutional doping.

3.4.3 Electronic and Magnetic Properties of WSe₂ with Vacancies

To calculate the electronic and magnetic properties of defected WSe$_2$, we will create vacancies at W sites and plot DOS and band structures of defected WSe$_2$. Several electronic and magnetic properties including bandgap values, formation energies, conductivities and magnetic moments are calculated.

Figures 31-34, and Figure 37 show the optimized structure with a single, three and four vacancies in the WSe$_2$ monolayer. A 6x6x1 supercell was used for the present study of the monolayer of defected WSe$_2$. Table 8 summarizes the results performed.
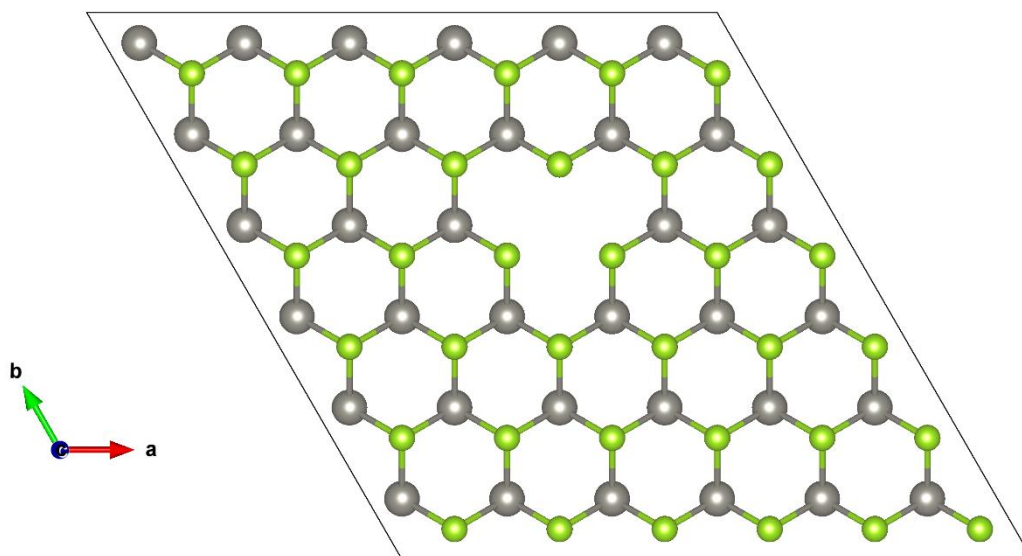
Figure 31: Top View of the 6 x 6 x 1 Supercell of the Pristine 2D WSe$_2$ Nanosheet with a Mono Vacancy (1 V)
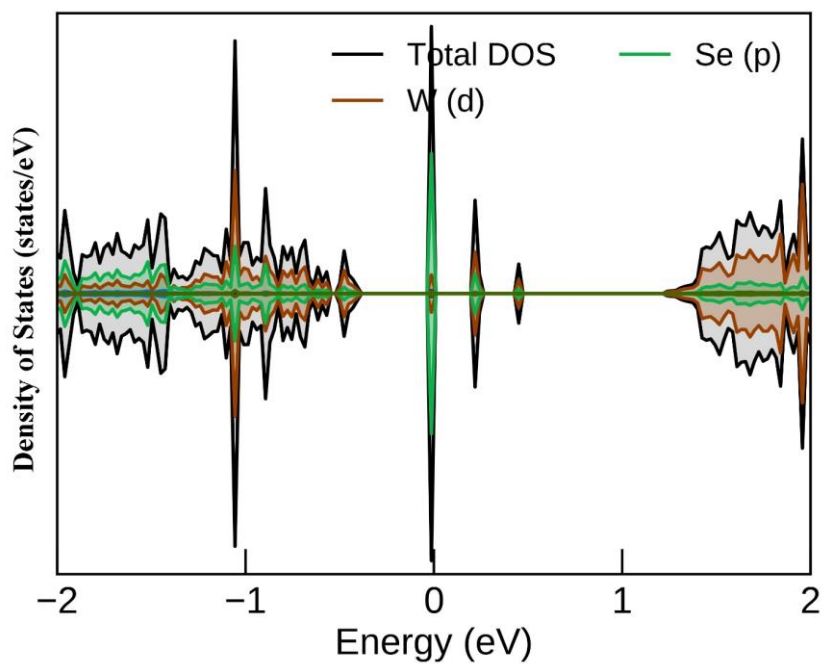
Figure 32: Total and Partial DOS of the 6 x 6 x 1 Supercell of the Defected 2D WSe$_2$ Material with a Mono Vacancy (1 V)
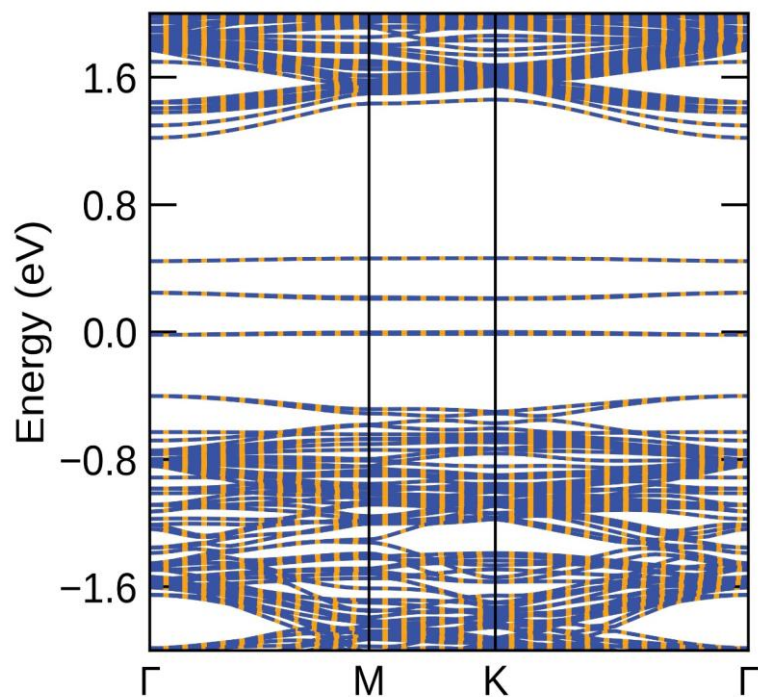
Figure 33: Band Structure of the 6 x 6 x 1 Supercell of the Defected 2D WSe$_2$ Material with a Mono Vacancy (1 V)
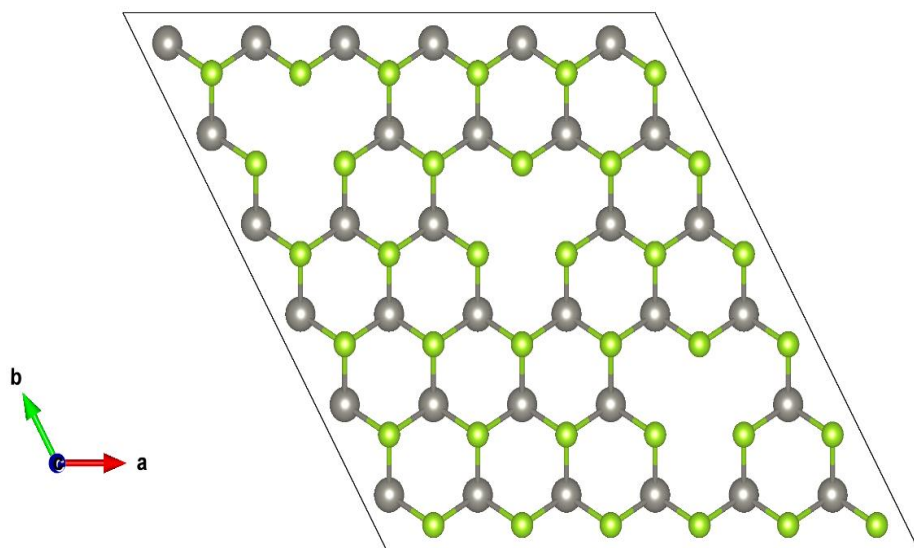
Figure 34: Top View of the 6 x 6 x1 Supercell 2D WSe$_2$ Nanosheet with Three Vacancies (3 V)
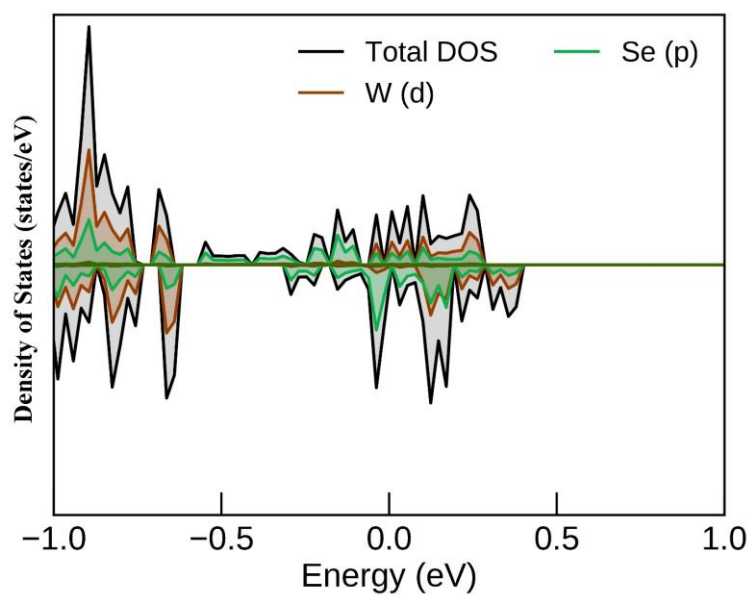
Figure 35: Total and Partial DOS of the 6 x 6 x 1 Supercell of the Defected 2D WSe$_2$ Material with Three Vacancies (3 V)
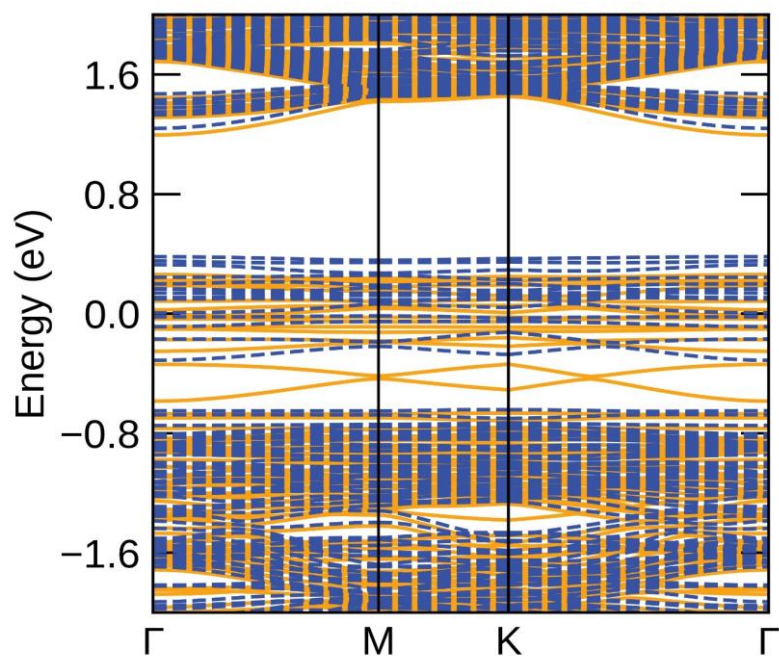
Figure 36: Band Structure of the 6 x 6 x 1 Supercell of the Defected 2D WSe$_2$ Material with Three Vacancies (3 V)
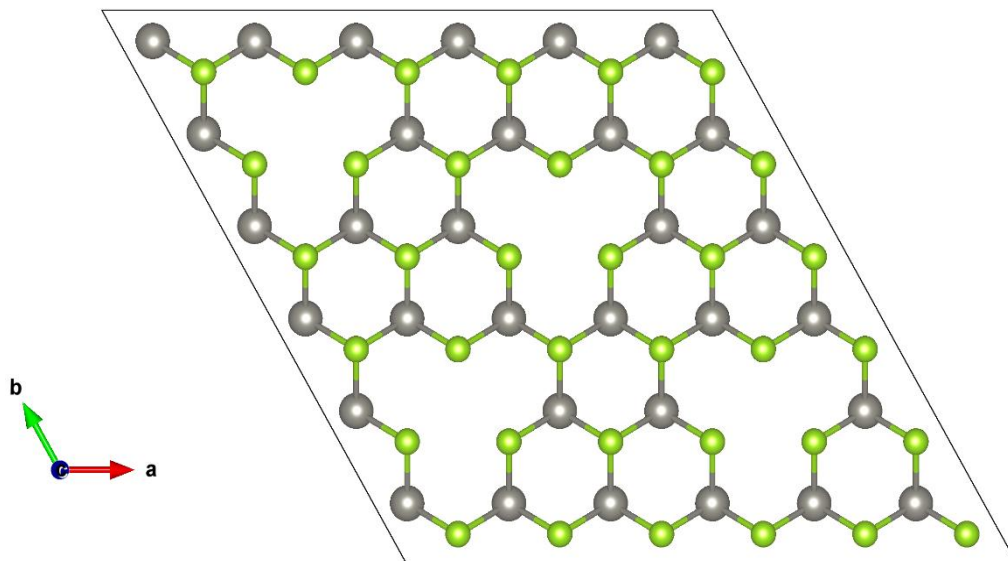
Figure 37: Top View of the 6 x 6 x 1 Supercell of the Defected 2D WSe$_2$ Nanosheet with Four Vacancies (4 V)
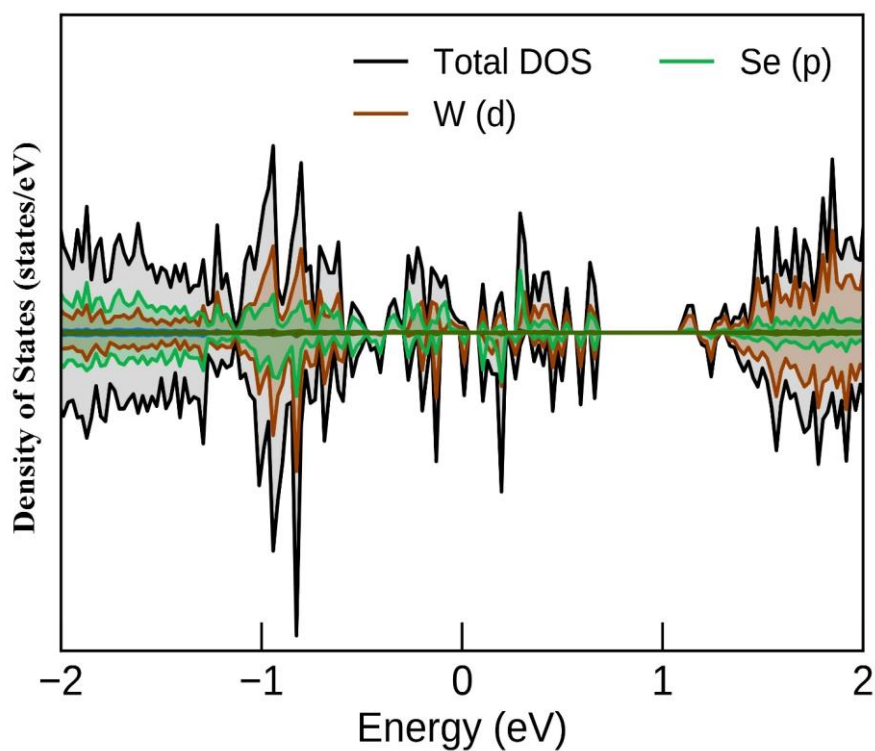
Figure 38: Total and Partial DOS of the 6 x 6 x 1 Supercell of the Defected 2D WSe$_2$ Material with Four Vacancies (4 V)
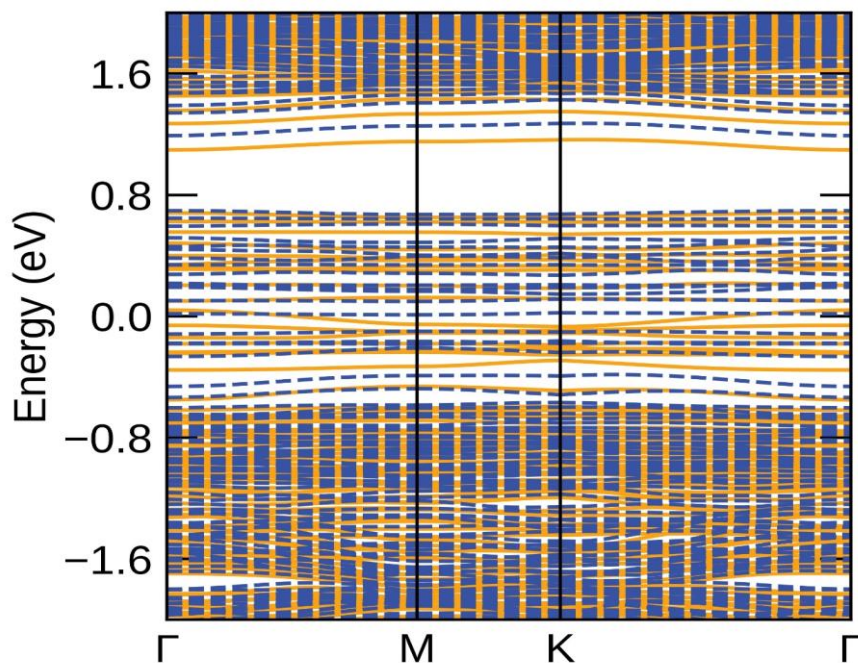
Figure 39: Band Structure of the 6 x 6 x 1 Supercell of the defected 2D WSe_2
Material with Four Vacancies (4 V)

Table 8: Summary of the Effect of Vacancy Defects in WSe_2 Monolayer

System	Formation Energy (eV/F.u.c)	Band Structure	Nature	Bandgap (eV)	Magnetic Moment (μ_B)
WSe_2	-0.578	Γ----Γ	Semiconductor	1.539	----
(1 V) WSe_2	5.122	K----M	Semiconductor	0.208	----
(3 V) WSe_2	15.216	-----	Metallic	-----	4.3987
(4 V) WSe_2	19.385	M----M	Nearly semi-metallic	0.0026 down	3.750

Figure 33 shows the electronic band structure of the single vacancy of WSe_2. As Table 8 shows, the defected monolayer remains to be semiconducting, but there are extra electronic states generated from the vacancy located at the bandgap area. As a result, the energy gap reduces to 0.208 eV from the pristine WSe_2 has a bandgap of 1.539 eV. Furthermore, creating three vacancies at the W site, makes it metallic and induces a

magnetic moment of 4.3987 μ_B. The band structure shows that spin up and spins channels have crossed the Fermi level indicating magnetic behaviour of defected WSe_2 and making it metallic. Figure 39 shows the band structure of defected WSe_2 with 4 vacancies at the W site. It is evident from the band structure that the bandgap reduced further to a value of 0.0026 eV and it shows a half-metallic character as the spin-up and spins down channel cross the Fermi level and the magnetic moment is 3.75 μ_B. Density Of State (DOS) were also calculated for the defected WSe_2 and is shown in Figures 32-35, and Figure 38 for the single, three and four vacancies. It is clear from Figure 33 that the substance is still a semiconductor, though the value of the bandgap has reduced.

The electronic states are mainly contributed by '*d*' orbitals in the conduction band around the vacancy and some contribution of p orbitals of Se atoms in the valance band around the vacancy which can be seen. Figure 35 shows the DOS of WSe_2 with three vacancies at the W site. DOS indicate the contribution of both d orbitals of W atoms and a little from the p orbitals of Se atoms at the conduction band crossing over the Fermi level and making it magnetic with a magnetic moment of 4.3987 μ_B. Figure 38 shows the DOS of WSe_2 with four vacancies. It shows a half-metallic character as the electronic states of d-orbitals of W and p-orbitals of Se crosses the Fermi level from the valence band and move to the conduction band.

3.5 Bandgap Tuning of the WSe₂ Through Substitutional Doping

Monolayer WSe_2 has a hexagonal crystal structure where W exists at the trigonal prismatic with six nearby Se atoms. A supercell of 6x6x1 dimension was created as shown in Figure 30 in which one W atom was replaced with one Rh and Ru atom with a doping concentration of 2.7%, 8.3% and 11.11% respectively. The geometrical

structure was relaxed and optimized before doping with TM atoms. The closing value of the ion radius of W with the TM dopants Rh and Ru suggest that there will be minimum distortion in the structure of doped TMD WSe_2.

3.5.1 Effects of Rh Doping on the Electronic and Magnetic Properties of the WSe_2 Monolayer

Figures 40-42, and Figure 44 show the band structure of Rh doped WSe_2 with 2.7%, 8.3% and 11.11% concentration, respectively. It is evident from Table 9 that as the doping as the concentration increases from 2.7% to 11.11%, the bandgap reduces from 1.539 eV to 0.20 eV which is a significant result, and it makes Rh a suitable candidate for bandgap tuning. Another outcome which is worth noting is the magnetic moment of 2.7% and 8.3% concentration of Rh doping induced a magnetic moment of 2.99 μ_B and 1.00 μ_B, respectively. Whereas 11.11% concentration does not bring the magnetic moment of the doped WSe_2. All the doped concentrations of Rh keep the semiconductor behaviour of doped WSe_2 intact.

Figures 41-43 and Figure 45 show the DOS of low, medium, and high Rh doped WSe_2. All the DOS plots show the main contribution of d-orbitals of W and Rh while some contribution of p-orbitals of Se atoms is also clear from the DOS. Medium doped Rh shows the main contribution of d orbitals of W and Rh while the little contribution of p and d orbitals of Se atoms is also noted.
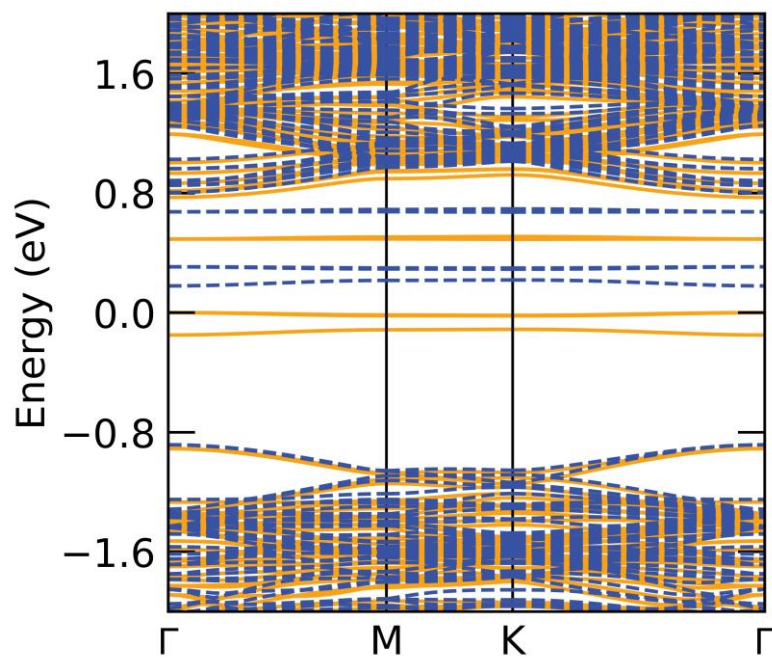
Figure 40: Band Structure of 2.7% Rh Doped WSe$_2$
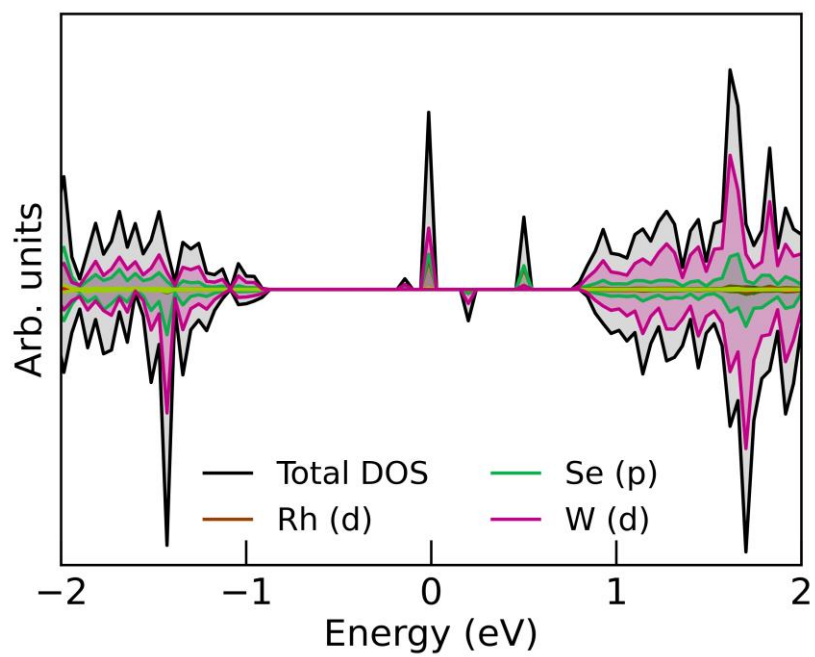
Figure 41: DOS of 2.7% Rh Doped WSe$_2$
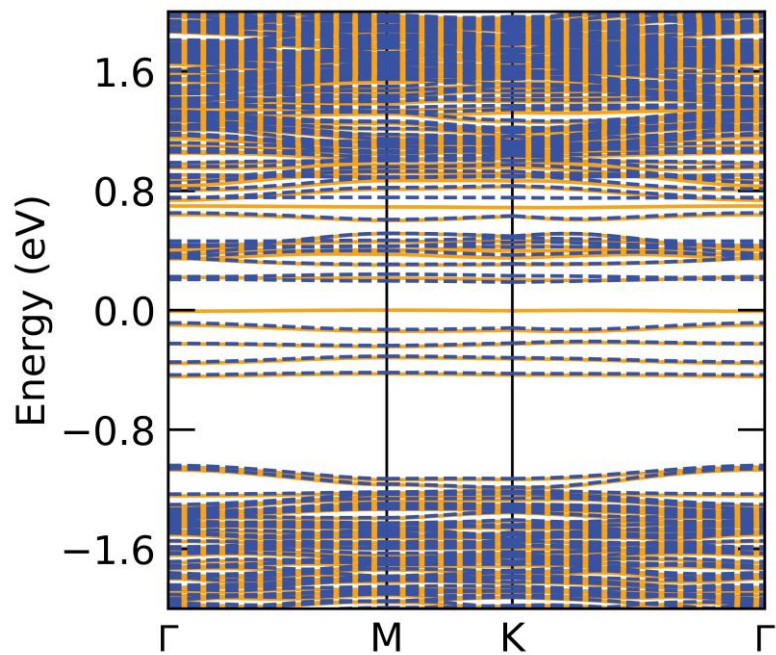
Figure 42: Band Structure of 8.3% Rh Doped WSe$_2$
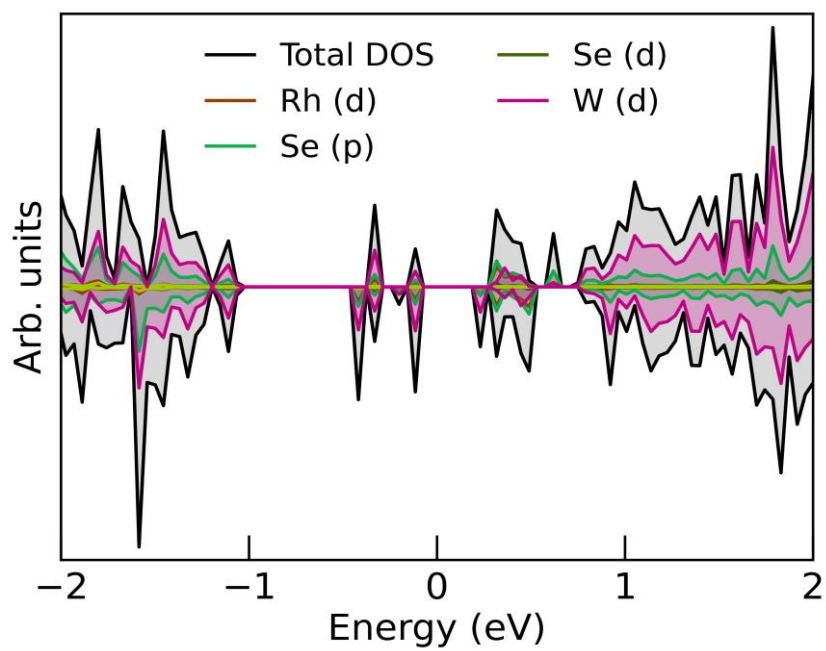
Figure 43: DOS of 8.3% Rh Doped WSe$_2$
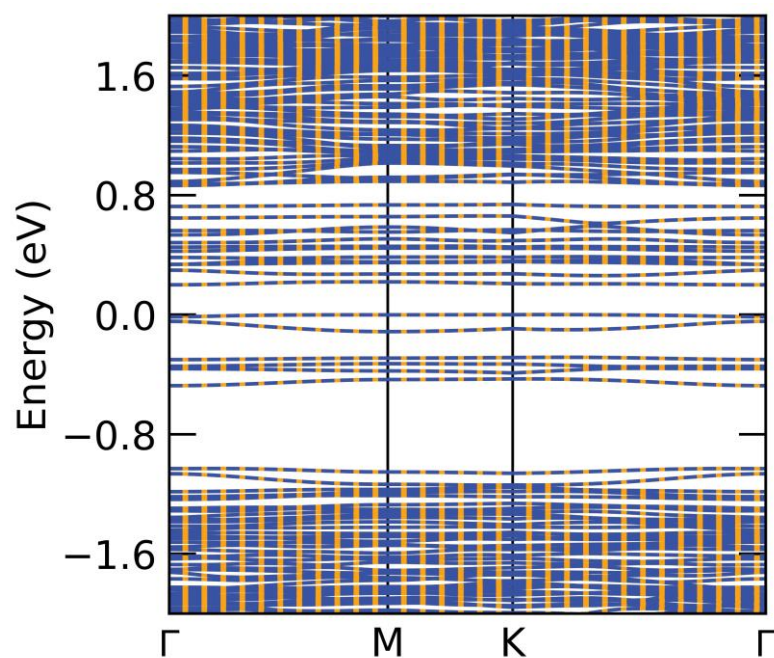
Figure 44: Band Structure of 11.11% Rh Doped WSe$_2$
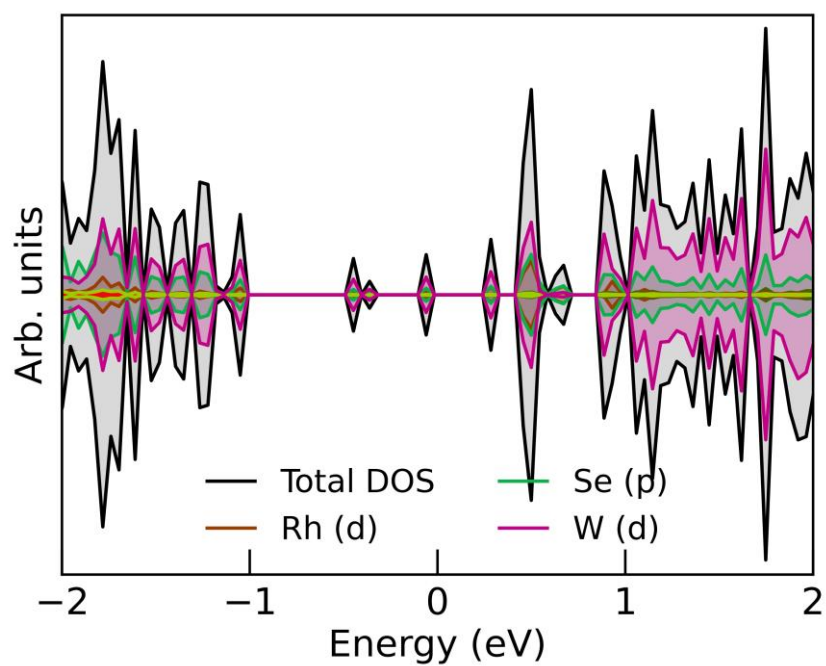
Figure 45: DOS of 11.11% Rh Doped WSe$_2$

Table 9: Summary of the Effect of Rh Doping in WSe_2 Monolayer

System	Formation Energy (eV)	Band Structure	Conductivity	Bandgap (eV)	Magnetic Moment (μ_B)
WSe_2	-0.578	Γ----Γ	Semiconductor	1.539	----
WSe_2 (2.7% Rh)	3.654	Γ----Γ	Semiconductor	0.492	2.9949
WSe_2 (8.3% Rh)	8.324	Γ----K	Semiconductor	0.183	1.000
WSe_2 (11.11% Rh)	10.477	Γ----Γ	Semiconductor	0.20	-----

Table 9 summarizes the results performed on Rh doped WSe_2. The bandgap values reduce as the concentration of the dopant increases. The calculated formation energies show that a lower concentration of Rh dopant is more thermodynamically stable. Rh dopant also induces magnetic moment as listed in Table 9.

3.5.2 Effects of Ru Doping on the Electronic and Magnetic Properties of the WSe₂ Monolayer

Figures 46-48, and Figure 50 show the band structure calculated for low, medium, and high concentrations of Ru doped WSe_2. A low concentration (2.7%) of Ru makes it half-metallic as shown in Figure 46 as the spin-up channel crosses the Fermi level and the spin-down channel does not.
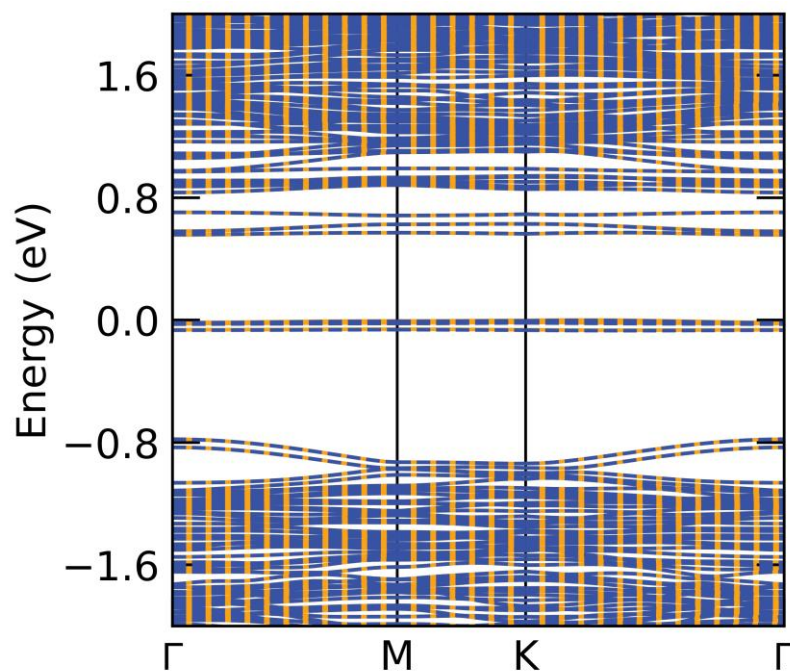
Figure 46: Band Structure of 2.7% Ru Doped WSe$_2$
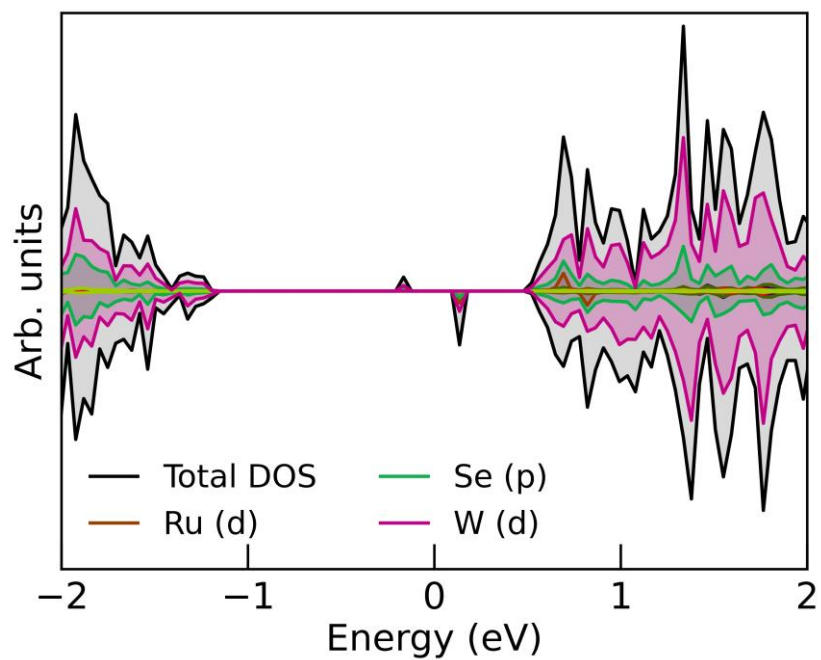
Figure 47: DOS of 2.7% Ru Doped WSe$_2$
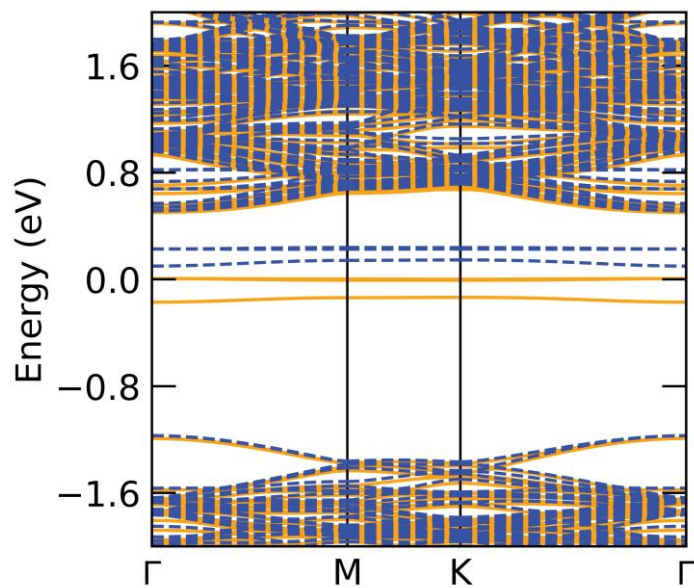
Figure 48: Band Structure of 8.3% Ru Doped WSe₂
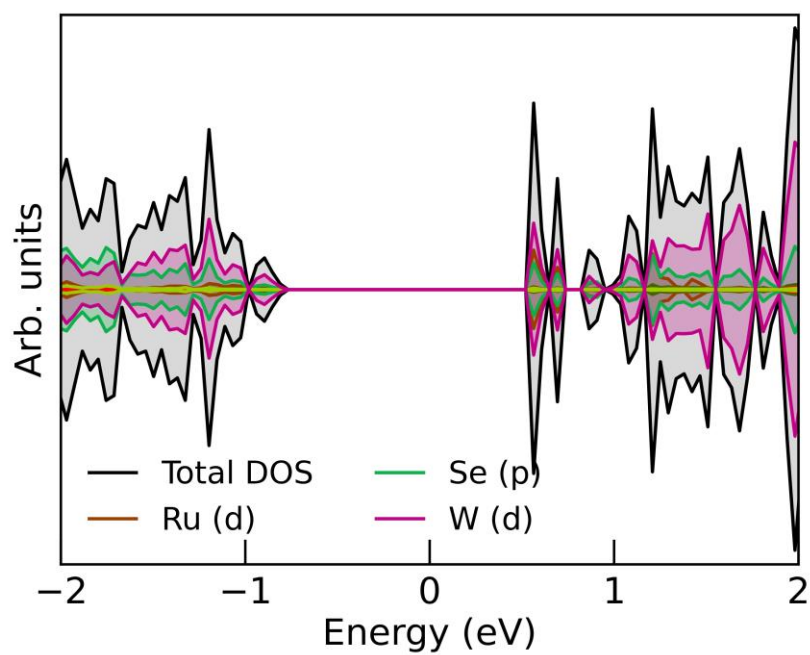
Figure 49: DOS of 2.7% Ru Doped WSe₂
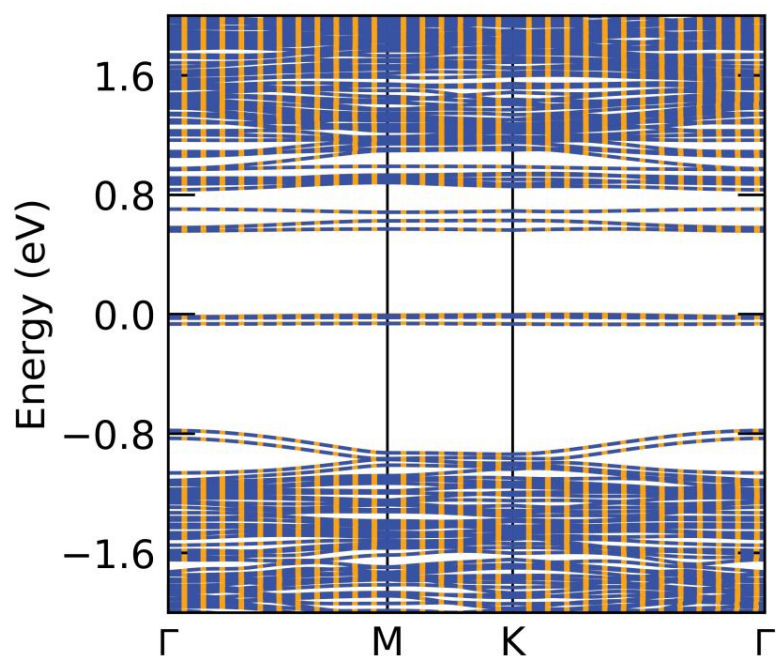
Figure 50: Band Structure of 11.11% Ru Doped WSe$_2$
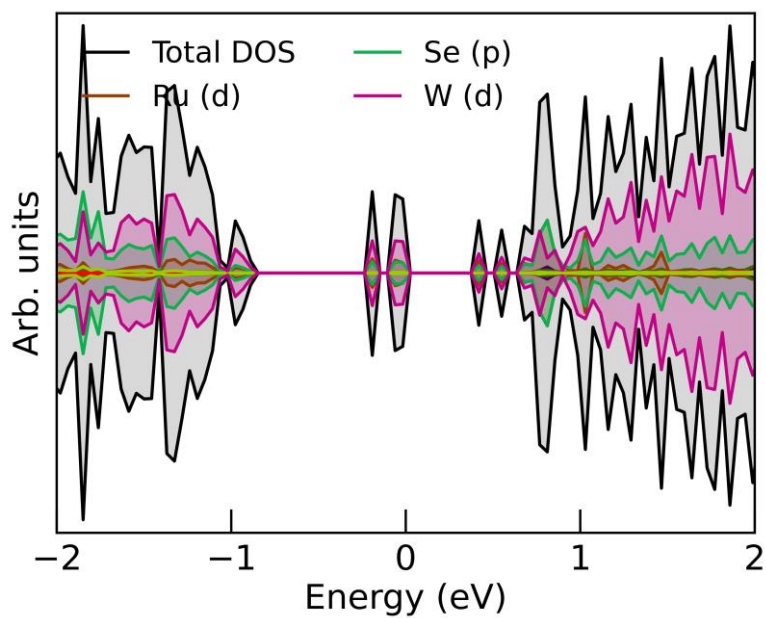
Figure 51: DOS of 2.7% Ru Doped WSe$_2$

Table 10: Summary of the Effect of Ru Doping on WSe$_2$ Monolayer

System	Formation Energy (eV)	Band Structure	Conductivity	Bandgap (eV)	Magnetic Moment (μ_B)
Pristine WSe$_2$	-0.578	Γ----Γ	Semiconductor	1.539	----
WSe$_2$ (8.3% Ru)	5.917	K---- Γ	Semiconductor	0.55	----
WSe$_2$ (11.11% Ru)	6.580	K---- Γ	Semiconductor	0.376	----
WSe$_2$ (2.7% Ru)	2.954	Γ----Γ	Semi-metallic	1.26 spin down	1.9786

Figures 47-49, and Figure 51 show the DOS of the low (2.7%), medium (8.3%) and high (11.11%), Ru doped WSe$_2$. It is clear from the DOS that 'd' orbitals contributed the most towards the electronic states while p orbitals of Se and d orbitals of Ru also contributed slightly. 2.7% Ru doped (low doping) resulted in a half-metallic character which is visible from the band structures shown in Figure 47. The spin-down channels have crossed the Fermi level inducing a magnetic moment of 1.9786 μ_B. Table 10 reveals the bandgap values calculated for the Ru doped WSe$_2$. Ru Doping into pristine WSe$_2$ reduced the bandgap from 1.539 eV to 0.376 eV depending on the different concentrations of Ru.11.11% Ru doped WSe$_2$ resulted in a maximum reduction in the bandgap though it's still showing semiconductor behaviour.

Formation Energy is calculated for all the doped systems of WSe$_2$, and it is clear from Tables 9-10 that formation energies increase as we increase the doping concentration of both Ru and Rh metals. Formation energy can be calculated by using the following equation.

$$E_{form} = E_{MX_2} - \sum n_i E_i \qquad \text{(Equation 3.1)}$$

Where E_{MX_2} is the energy of monolayer MX_2 per unit cell, i is the element that constitutes MX_2, n_i is the number of i atom per unit cell, and E_i is the energy of the i atom. The formation energy of the defects was $E_{form-defect}$ for the defect of monolayer MX_2 were calculated as:

$$E_{form-defect} = E_{MX_2-defect} + \sum n_i E_i - n_j E_j - E_{MX_2} \qquad \text{(Equation 3.2)}$$

Where $E_{MX_2-defect}$ and E_{MX_2} are the total energy of the 6x6x1 supercell of monolayer MX_2 with and without defect, respectively i and j are removed and added elements in MX_2, n_i and n_j are the number of removed i and added j atom, E_i and E_j are the energy of the i and j atoms. Negative formation energy shows a more thermodynamically stable configuration. Hence, we notice in Table 8 that as the number of vacancies in WSe$_2$ increases, the formation energy increases from 5.122 eV to 19.385 eV.

We see a decrease in the formation energy once we dope it with Ru and Rh metals showing thermodynamically more stability with an increased concentration of doping. It is also noticeable that Ru is thermodynamically more favourable and stable than Rh doping.

The results obtained in this chapter are very extensive and have sufficient data to explore the bandgap tuning of WSe$_2$ and MoSe$_2$. The effects will be analysed in detail in the next chapter of the discussion.

Chapter 4: Discussion

The results listed in the earlier chapter highlight the electronic and magnetic properties of both $MoSe_2$ and WSe_2. They include Bandgap values, formation energy, magnetic moments supported by the band structure plots and DOS of both pristine and doped $MoSe_2$ and WSe_2.

4.1 Comparison between Pristine $MoSe_2$ and WSe_2

Table 2 lays out some of the earlier research performed and compares it with this work. It is reported that the bandgap value calculated for pristine $MoSe_2$ by different experimental and theoretical methods as listed in Table 2 is very close to the calculated value of 1.432 eV using the GGA method in this research. Our results in Table 2 verify $MoSe_2$ as a semiconductor with a direct bandgap at the Γ position and the formation energy calculated value is -0.725 eV. Whereas Table 8 shows results calculated for pristine WSe_2 that confirm it as a semiconductor with a direct bandgap value of 1.539 eV and formation energy of -0.578 eV. The comparison of the following sections between the $MoSe_2$ and WSe_2 will be laid out, discussing the effects of vacancy creation, and doping, respectively.

4.2 Comparison between $MoSe_2$ and WSe_2 with Vacancy

Table 3 summarizes the effects of vacancy creation on $MoSe_2$ semiconductors. It shows how mono vacancy creation decreases the bandgap value significantly from 1.432 eV to 0.089 eV proving that vacancy creation is a successful method for bandgap tuning. Furthermore, it is clear from the results in Table 3 that as the number of vacancies increases, the bandgap value decreases so. It is calculated that tri vacancies make $MoSe_2$ metallic while introducing Penta vacancies reduces the bandgap further to 0.029 eV.

Results are also calculated for the formation energies in Table 5 showing an increase in formation energies for pristine $MoSe_2$ from -0.725 eV to 22.758 eV showing that a lower number of vacancies are thermodynamically suitable for the system. Table 4 summarizes the results of calculated magnetic moments on $MoSe_2$ after mono, tri, and Penta vacancies creation. It reveals that magnetic moment increases first from 3.999 μ_B to 12.000 μ_B after creating mono to tri vacancies but it reduced to a value of 2.00 μ_B after creating five vacancies in $MoSe_2$.

Table 8 summarizes the results of vacancy creation in WSe_2 semiconductors showing the formation energies and bandgap values. Table 8 shows that the pristine WSe_2 has a bandgap value of 1.539 eV, and it reduces significantly to 0.0026 eV for mono to Penta vacancies making it a suitable method of bandgap engineering. Related results are listed for the formation energies in Table 8 which display the formation energy of pristine WSe_2 as -0.587 eV which increases to 19.385 eV after introducing mono to Penta vacancies proving that the small number of vacancies is favourable for thermodynamically stable WSe_2.Magnetic moments are also calculated for the defected WSe_2, and Table 8 shows the results. Magnetic moment decreases from 4.9387 μ_B to 3.750 μ_B for tri to Penta vacancies showing that a higher number of vacancies create a lower magnetic moment.

4.3 Comparison between Doped $MoSe_2$ and WSe_2

Calculations were performed on the pristine sample of $MoSe_2$ and WSe_2 with various concentrations of Ru and Rh metals. They have been labelled as low, medium, and high accordingly as the concentration level increases. Where low (2.7%), medium (8.3%), high is (13.88%) for $MoSe_2$ and for WSe_2, low is (2.7%), medium is 8.3% and High is (11.11%). Both the metals turn out to be a useful source of bandgap tuning and

the results are listed in chapter 3, Tables 6-7, and Tables 9-10. It is clear from the conducted research in Table 6, that conductivity of Rh doped $MoSe_2$ changes as the concentration of the doped metal changes. It shows a semiconductor behaviour with 2.7% and 13.88% concentration of Rh doping while it reveals a semimetal tendency for 8.3% doping.

The calculated bandgaps are also listed in Table 6 which proves Rh to be a useful source of bandgap tuning as the bandgap reduces from 0.568 eV to 0.022 eV for low to a high concentration of Rh in pristine $MoSe_2$. Furthermore, Table 6 details the calculated magnetic moments of the Rh doped $MoSe_2$ as well. It is shown from the results that magnetic moment increases from 2.98 μ_B to 8.93 μ_B as the concentration of Rh doping increases from 2.7% to 8.3% but then reduces to 1.002 μ_B as the concentration increases further to a 13.8%. Table 6 shows the formation energies of Rh doped $MoSe_2$. It is reported after the calculations that formation energies increase from -1.721 eV to 9.050 eV as the dopant concentration of Rh increases in $MoSe_2$. That makes a low concentration of Rh thermodynamically favourable.

Table 7 summarizes the results of formation energies, bandgap transition, bandgap values and magnetic moments for Ru doped $MoSe_2$.Bandgap values reduce significantly from 1.432 eV for pristine $MoSe_2$ to 0.271 eV for a high concentration of Ru metal doping. It proves that Ru transition metal is a practical choice for bandgap engineering. Table 7 list the magnetic moments of the Ru doped $MoSe_2$ as well. A low concentration (2.7%) of Ru doping results in a magnetic moment of 2.00 μ_B and it increases to 4.53 μ_B as the doping concentration rises to a 13.8% value. AS per the conductivity is concerned, a low concentration (2.7%) of Ru metal results in a half-metallic character while the medium (8.3%) and high concentration (13.88%) of Ru

doping result in a semiconductor nature. Formation energies listed in Table 7 shows an increase from -0.2367 eV to 6.931 eV as the concentration of Ru increases from 2.7% to 13.88% in MoSe$_2$. Low values of formation energies depict a more thermodynamically stable system hence the low concentration (2.7%) of Ru dopant is more favourable than high concentrations (13.88%).

Table 10 summarizes the effects of Ru doping on WSe$_2$. It tabulates formation energies, conductivities, bandgap values and magnetic moments. It is evident from Table 10 that the bandgap reduces from 1.539 eV for pristine WSe$_2$ to 0.492 eV for a low concentration (2.7%) of Ru doping. As the concentration increases from medium (8.3 %) to high (11.11%) its value increases slightly from 0.183 eV to 0.2 eV. Magnetic moment decreases from 2.99 μ_B to 1.000 μ_B as the dopant concentration increased from medium (8.3%) to high (11.11%). Our DFT calculations show formation energies of pristine WSe$_2$ as -0.578 eV while it increases from 3.654 eV to 10.477 eV for low (2.7%) to high concentration (11.11%) of Ru doping in WSe$_2$, respectively.

As per conductivity is concerned, Table 10 shows that WSe$_2$ keeps its semiconductor character even after doping with a medium and high concentration of Ru and as well as with low, high, and medium concentrations of Rh dopant. It shows a half-metallic nature with a low concentration of TM Ru as listed in Table 10.

It shows calculations for formation energies, bandgap values, magnetic moments, and conductivity status. It is clear from the results that the bandgap values reduce from 1.539 eV to 1.26 eV for pristine WSe$_2$ to 2.7% Ru doped WSe$_2$. It further reduces to a value of 0.55 eV for medium concentration (8.3%) of Ru and it reduces to 0.376 eV for high concentration (11.11%) of Ru. It makes Ru metal a favourable candidate for bandgap reduction. The magnetic moment calculated for a low concentration (2.7%)

of Ru doping in WSe_2 resulted in 1.978 μ_B. Formation energies are also calculated, and formation energies increase from 2.954 eV to 6.58 eV as the dopant concentration increases from low (2.7%) to high (11.11%). It suggests that a low concentration (2.7%) of Ru is thermodynamically more suitable as compared to other systems in which Ru concentration is medium (8.3%) or high (11.11%).

Our discussion analysed the results obtained during the research and both methods supply ways for successful bandgap tuning. During the process, it is discovered that the metallic character of WSe_2 and $MoSe_2$ is visible for tri vacancies. Furthermore, bandgap reduces as we increase the dopant concentration and the number of vacancies in both the compounds.

Chapter 5: Conclusion

In summary, first-principles calculation of 3d transition metal Rh, Ru doped $MoSe_2$ and WSe_2 monolayer are performed to study their electronic and magnetic properties. The results show that the doped system maintains the structure type of monolayered $MoSe_2$ and WSe_2. Furthermore, this research also focused on bandgap tuning of $MoSe_2$ and WSe_2 monolayers by creating vacancies. Both the methods are successful in terms of lowering the bandgap values.

The calculated formation energies show that the incorporation of TM impurities is energetically preferable under Rh dopant in $MoSe_2$ as the formation energies are lower i.e., -1.732 eV for 2.7% concentration of Rh while For WSe_2 the low formation energies are calculated 2.954 eV for Ru dopant for 2.7% concentration. For vacancy creation, it is found that WSe_2 has low formation energy i.e., 5.122 eV for the mono vacancy as compared to $MoSe_2$ where it is 5.781 eV for the mono vacancy.

As far as bandgap values are concerned, WSe_2 shows more reduction in bandgap values than $MoSe_2$ as the number of vacancies increases. In WSe_2 the bandgap reduces from 1.539 eV to 0.0026 eV whereas, in $MoSe_2$ the bandgap reduces from 1.432 eV to 0.029 eV. While regarding TM dopants, $MoSe_2$ shows lower values of bandgap i.e., 0.022 eV with high concentration (13.8%) of Rh than Ru where it reduces the bandgap to 0.271 eV. A similar trend is followed in WSe_2 where Rh dopant reduced the value of bandgap to 0.20 eV and Ru dopant lowered it reduces to 0.376 eV which is 12% more hence Rh dopant is more successful when it comes to bandgap tuning.

In addition, the spin-polarized calculations say the magnetic behaviour of the studied WSe_2 and $MoSe_2$ monolayers by both strategies i.e., by doping of transition metals

(Ru & Rh) as well as by creating vacancies. With regards to MoSe$_2$, magnetic moment increases from 3.99 μ_B to 12.00 μ_B for mono to tri vacancies and then decreases to 2.00 μ_B with the introduction of Penta vacancies. Also, with the inclusion of TM Rh dopant, the magnetic moment increases from 2.9799 μ_B to 8.9235 μ_B for 2.7% concentration of dopant to 8.3% and then further decreases to 1.002 μ_B by increasing the concentration to 13.8%. Whereas magnetic moment increases from 2.00 μ_B to 4.33 μ_B by adding Ru impurity from 2.7% to 13.8% concentration and shows a semiconductor behaviour for 8.3% concentration of Ru dopant.

Regarding WSe$_2$, it shows semiconductor behaviour with the mono vacancy and shows metallic behaviour with tri vacancies and nearly half-metallic with four vacancies. With Ru dopant, WSe$_2$ shows the half-metallic character with a low concentration of 2.7% and a magnetic moment of 1.978 μ_B and then it further shows semiconductor tendency by increasing the concentration of Ru from 8.3% to 11.11%. In addition to TM Rh as a dopant in WSe$_2$, it shows and decreases in the magnetic moment from 2.99 μ_B to 1.00 μ_B as the concentration increases from 2.7% to 8.3% but WSe$_2$ exhibits a semiconducting behaviour as concentration increases further to 11.11%.

Concerning conductivity, both WSe$_2$ and MoSe$_2$ show different behaviour under different conditions which include semiconducting, half-metallic and metallic characteristics. For MoSe$_2$, tri vacancies show a metallic character and mono and Penta vacancies give the semiconductor nature of MoSe$_2$. For low concentration (2.7%) of Ru, it shows half-metallic nature and semiconductor behaviour for (8.3%) and (13.88%) of Ru.

The medium concentration (8.3%) of Rh exhibits a half-metallic behaviour while for 2.7% and 13.88% of doped Rh, MoSe$_2$ shows a semiconductor nature. When it comes

to WSe$_2$, the half-metallic character is found for low concentration (2.7%) of Ru and nearly half-metallic with four vacancies. Tri vacancies creation results in the metallic character of WSe$_2$.Semiconducting nature is revealed for the rest of the configurations as listed in Tables 9-10.

Another interesting finding of the research are the nature of the bandgap whether is direct or indirect. It is found that some configuration shows direct bandgap which includes pristine MoSe$_2$ where the bandgap transition happens at the Γ-point showing direct bandgap. For mono vacancy, it has a direct bandgap Γ-points and for Penta vacancies, it occurs at K- Γ points showing an indirect bandgap. Also, low (2.7%), and high concentration (13.88%) of Ru shows the direct bandgap at Γ-point and indirect bandgap at M---Γ points for medium concentration (8.3%) of Ru. Similar findings are reported for Rh in the research where 2.7% and 13.8% of Rh concentration reveal direct bandgaps at Γ points in MoSe$_2$ while it shows indirect bandgap for medium concentration 8.3% of Rh at M----Γ points. For WSe$_2$, results show that the pristine form of WSe$_2$ has a direct bandgap at Γ- point while low (2.7%) and high (11.11%) Rh concentration of impurity also results in direct bandgap at Γ- point. For Ru dopant, a low concentration of (2.7%) results in a direct bandgap at Γ-point and medium (8.3%) and a high (11.11%) concentration of Ru results in an indirect bandgap at K----Γ points. It is interesting to find that four vacancies in WSe$_2$ indicate a direct bandgap at M-point while mono vacancy results in an indirect bandgap at K----M points.

In conclusion, our results reveal that bandgap values reduce linearly in both semiconductors with an increase in the number of vacancies and with an increased concentration of dopants. Also, magnetism is induced in both compounds with the two methods of bandgap tuning. The transition from semiconductor to metals and half

metal is also recorded in both compounds using the specified ways of bandgap tuning. Another finding of the research is that doped systems are more thermodynamically favourable than the ones with vacancies as revealed by the values of formation energies.

5.1 Research Implications

Our results reveal that 3d TM doping and vacancy creation is an effective method for modulating the electronic properties of $MoSe_2$ and WSe_2 monolayers which can be used for making nanodevices for electronic, optical and spintronics applications. It will open doors for research in the electronic industry locally and contribute valuably to the international scientific community.

References

Ahmed, S., Ding, X., Murmu, P. P., Bao, N., Liu, R., Kennedy, J., ..., & Yi, J. (2020). High coercivity and magnetization in WSe$_2$ by codoping Co and Nb. *Small*, *16*(12), 1903173. https://doi.org/10.1002/smll.201903173

Ataca, C., Sahin, H., & Ciraci, S. (2012). Stable, single-layer MX2 transition-metal oxides and dichalcogenides in a honeycomb-like structure. *The Journal of Physical Chemistry C*, *116*(16), 8983-8999. https://doi.org/10.1021/jp212558p

Bhimanapati, G. R., Lin, Z., Meunier, V., Jung, Y., Cha, J., Das, S., ..., & Robinson, J. A. (2015). Recent advances in two-dimensional materials beyond graphene. *ACS Nano*, *9*(12), 11509-11539
https://doi.org/10.1021/acsnano.5b05556

Born, M., & Heisenberg, W. (1985). Zur Quantentheorie der Molekeln. In *Original Scientific Papers Wissenschaftliche Originalarbeiten* (pp. 216-246). Springer, Berlin, Heidelberg. https://doi.org/10.1007/978-3-642-61659-4_16

Cheiwchanchamnangij, T., & Lambrecht, W. R. J. P. R. B. (2012). Quasiparticle band structure calculation of monolayer, bilayer, and bulk MoS$_2$. *85*(20), 205302. https://doi.org/10.1103/PhysRevB.85.205302

Choi, W., Choudhary, N., Han, G. H., Park, J., Akinwande, D., & Lee, Y. H. (2017). Recent development of two-dimensional transition metal dichalcogenides and their applications. *Materials Today*, *20*(3), 116-130
https://doi.org/10.1016/j.mattod.2016.10.002

Coehoorn, R., Haas, C., Dijkstra, J., Flipse, C. D., De Groot, R. A., & Wold, A. (1987). Electronic structure of MoSe$_2$, MoS$_2$, and WSe$_2$. I. Band-structure calculations and photoelectron spectroscopy. *Physical Review B*, *35*(12), 6195. https://doi.org/10.1103/PhysRevB.35.6195

Daukiya, L., Seibel, J., & De Feyter, S. (2019). Chemical modification of 2D materials using molecules and assemblies of molecules. *Advances in Physics: X*, *4*(1), 1625723. https://doi.org/10.1080/23746149.2019.1625723

Deng, S., Li, L., & Zhang, Y. (2018). Strain modulated electronic, mechanical, and optical properties of the monolayer PdS2, PdSe2, and PtSe$_2$ for tunable devices. *ACS Applied Nano Materials*, *1*(4), 1932-1939
https://doi.org/10.1021/acsanm.8b00363

Diez-Perez, I., Li, Z., Guo, S., Madden, C., Huang, H., Che, Y., ... & Tao, N. (2012). Ambipolar transport in an electrochemically gated single-molecule field-effect transistor. *ACS nano*, *6*(8), 7044-7052. https://doi.org/10.1021/nn302090t

Donaldson, L. (2019). New class of 2D material could improve quantum computing. *Materials Today, 29*, 2-3 https://doi.org/10.1016/j.mattod.2019.07.014

Eberhard, E., & Dreizler, R. (2011). Foundations of density functional theory: Existence theorems. In *Density Functional Theory. An Advanced Course* (pp.11-56). Berlin: Springer https://doi.org/10.1007/978-3-642-14090-7_2

Fang, H., Chuang, S., Chang, T. C., Takei, K., Takahashi, T., & Javey, A. (2012). High-performance single layered WSe_2 p-FETs with chemically doped contacts. *Nano Letters*, *12*(7), 3788-3792. https://doi.org/10.1021/nl301702r

Garnier, F., Hajlaoui, R., Yassar, A., & Srivastava, P. (1994). All-polymer field-effect transistor realized by printing techniques. *Science*, *265*(5179), 1684-1686. https://doi.org/10.1126/science.265.5179.1684

Liang, L., Wang, J., Lin, W., Sumpter, B. G., Meunier, V., & Pan, M. (2014). Electronic bandgap and edge reconstruction in phosphorene materials. *Nano letters*, *14*(11), 6400-6406. https://doi.org/10.1021/nl502892t

Habib, M. R., Wang, S., Wang, W., Xiao, H., Obaidulla, S. M., Gayen, A., ..., & Xu, M. (2019). Electronic properties of polymorphic two-dimensional layered chromium disulphide. *Nanoscale*, *11*(42), 20123-20132 https://doi.org/10.1039/C9NR04449C

Hamann, D. R., Schlüter, M., & Chiang, C. (1979). Norm-conserving pseudopotentials. *Physical Review Letters*, *43*(20), 1494 https://doi.org/10.1103/PhysRevLett.43.1494

Hartree, D. R. (1928, July). The wave mechanics of an atom with a non-coulomb central field. part iii. term values and intensities in series in optical spectra. In *Mathematical Proceedings of the Cambridge Philosophical Society*, *24*(3), 426-437. https://doi.org/10.1017/S0305004100015954

Hohenberg, P., & Kohn, W. (1964). Inhomogeneous electron gas. *Physical Review*, *136*(3B), B864. https://doi.org/10.1103/PhysRev.136.B864

Huang, B., Clark, G., Navarro-Moratalla, E., Klein, D. R., Cheng, R., Seyler, K. L., ..., & Xu, X. (2017). Layer-dependent ferromagnetism in a van der Waals crystal down to the monolayer limit. *Nature*, *546*(7657), 270-273 https://doi.org/10.1038/nature22391

Island, J. O., Kuc, A., Diependaal, E. H., Bratschitsch, R., Van Der Zant, H. S., Heine, T., & Castellanos-Gomez, A. (2016). Precise and reversible band gap tuning in single-layer $MoSe_2$ by uniaxial strain. *Nanoscale*, *8*(5), 2589-2593. https://doi.org/10.1039/C5NR08219F

Jain, A., Sadan, M. B., & Ramasubramaniam, A. (2020). Promoting active sites for hydrogen evolution in MoSe$_2$ via transition-metal doping. *The Journal of Physical Chemistry C*, *124*(23), 12324-12336 https://doi.org/10.1021/acs.jpcc.0c00013

Jia, B. (2019). 2D optical materials and the implications for photonics. *APL Photonics*, *4*(8), 080401. https://doi.org/10.1063/1.5120030

Jin, W., Yeh, P. C., Zaki, N., Zhang, D., Sadowski, J. T., Al-Mahboob, A., ... & Osgood Jr, R. M. (2013). Direct measurement of the thickness-dependent electronic band structure of MoS$_2$ using angle-resolved photoemission spectroscopy. *Physical Review Letters*, *111*(10), 106801 https://doi.org/10.1103/PhysRevLett.111.106801

Kam, K. K., & Parkinson, B. A. (1982). Cs. *The Journal of Physical Chemistry*, *86*(4), 463-467. https://doi.org/10.1021/j100393a010

Kohanoff, J., & Gidopoulos, N. I. (2003). Density functional theory: basics, new trends and applications. *Handbook of molecular physics and quantum chemistry*, *2*(Part 5), 532-568

Kohn, W., & Sham, L. J. (1965). Self-consistent equations including exchange and correlation effects. *Physical review*, *140*(4A), A1133 https://doi.org/10.1103/PhysRev.140.A1133

Kuc, A., Heine, T., & Kis, A. J. M. b. (2015). Electronic properties of transition-metal dichalcogenides. *40*(7), 577-584. https://doi.org/10.1039/C5CS00507H

Kumar, A., & Ahluwalia, P. K. (2012). Electronic structure of transition metal dichalcogenides monolayers 1H-MX2 (M= Mo, W; X= S, Se, Te) from ab-initio theory: new direct band gap semiconductors. *The European Physical Journal B*, *85*(6), 1-7. https://doi.org/10.1140/epjb/e2012-30070-x

Kumar, S., & Schwingenschlogl, U. (2015). Thermoelectric response of bulk and monolayer MoSe$_2$ and WSe$_2$. *Chemistry of Materials*, *27*(4), 1278-1284. Lee, H., Paeng, K., & Kim, I. S. (2018). A review of doping modulation in graphene. *Synthetic Metals*, *244*, 36-47. https://doi.org/10.1021/cm504244b

Lee, H., Paeng, K., & Kim, I. S. (2018). A review of doping modulation in graphene. *Synthetic Metals*, *244*, 36-47 https://doi.org/10.1016/j.synthmet.2018.07.001

Li, H., Huang, S., Zhang, Q., Zhu, Z., Li, C., Meng, J., & Tian, Y. (2018). Nonmetal doping induced electronic and magnetic properties in MoSe$_2$ monolayer. *Chemical Physics Letters*, *692*, 69-74 https://doi.org/10.1016/j.cplett.2017.12.010

Li, H., Wu, J., Yin, Z., & Zhang, H. (2014). Preparation and applications of mechanically exfoliated single-layer and multilayer MoS_2 and WSe_2 nanosheets. *Accounts of chemical research*, *47*(4), 1067-1075 https://doi.org/10.1021/ar4002312

Li, Q. L., Wang, L. L., Wang, X., Wang, M. L., & Zhao, R. S. (2016). Magnetic metal-organic nanotubes: an adsorbent for magnetic solid-phase extraction of polychlorinated biphenyls from environmental and biological samples. *Journal of Chromatography A*, *1449*, 39-47 https://doi.org/10.1016/j.chroma.2016.04.060

Li, Y., Qian, F., Xiang, J., & Lieber, C. M. (2006). Nanowire electronic and optoelectronic devices. *Materials Today*, *9*(10), 18-27 https://doi.org/10.1016/S1369-7021(06)71650-9

Li, Y., Rao, Y., Mak, K. F., You, Y., Wang, S., Dean, C. R., & Heinz, T. F. (2013). Probing Symmetry Properties of Few-Layer MoS_2 and h-BN by Optical Second-Harmonic Generation. *Nano Letters*, *13*(7), 3329-3333 https://doi.org/10.1021/nl401561r

Lin, X., & Ni, J. (2016). Magnetism and electronic phase transitions in monoclinic transition metal dichalcogenides with transition metal atoms embedded. *Journal of Applied Physics*, *120*(6), 064305 https://doi.org/10.1063/1.4960717

Liu, Y., Zhang, S., He, J., Wang, Z. M., & Liu, Z. (2019). Recent progress in the fabrication, properties, and devices of heterostructures based on 2D materials. *Nano-Micro Letters*, *11*(1), 1-24. https://doi.org/10.1007/s40820-019-0245-5

M Santhosh, N., Filipič, G., Kovacevic, E., Jagodar, A., Berndt, J., Strunskus, T., ... & Cvelbar, U. (2020). N-graphene nanowalls via plasma nitrogen incorporation and substitution: The experimental evidence. *Nano-micro letters*, *12*(1), 1-17. https://doi.org/10.1007/s40820-020-0395-5

Mabelet, L. B., Malonda-Boungou, B. R., Mabiala-Poaty, H. B., Raji, A. T., & M'Passi-Mabiala, B. (2020). Energetics, electronic and magnetic properties of monolayer WSe_2 doped with pnictogens, halogens and transition-metal (4d, 5d) atoms: An ab-initio study. *Physica E: Low-dimensional Systems and Nanostructures*, *124*, 114161. https://doi.org/10.1016/j.physe.2020.114161

Medvedev, M. G., Bushmarinov, I. S., Sun, J., Perdew, J. P., & Lyssenko, K. A. (2017). Density functional theory is straying from the path toward the exact functional. *Science*, *355*(6320), 49-52 https://doi.org/10.1126/science.aah5975

Morgan, H., Rout, C. S., & Late, D. J. (2019). Future prospects of 2D materials for sensing applications. In *Fundamentals and Sensing Applications of 2D Materials* (pp. 481-482). London: Woodhead Publishing. http://dx.doi.org/10.1016/B978-0-08-102577-2.00014-2

Nair, R. R., Sepioni, M., Tsai, I. L., Lehtinen, O., Keinonen, J., Krasheninnikov, A. V., ... & Grigorieva, I. V. (2012). Spin-half paramagnetism in graphene induced by point defects. *Nature Physics*, *8*(3), 199-202. https://doi.org/10.1038/nphys2183

Neto, A. C., Guinea, F., Peres, N. M. R., Novoselov, K. S., & Geim, A. K. (2009). The electronic properties of graphene, *Reviews of Modern Physics, 81*, 109. https://doi.org/10.1103/RevModPhys.81.109

Kitko, K. E. (2018). *Nanomaterial-Based Approaches to the Study Of Membrane Signaling* (Doctoral dissertation, Vanderbilt University, USA)

Novoselov, K. S., Geim, A. K., Morozov, S. V., Jiang, D. E., Zhang, Y., Dubonos, S. V., ..., & Firsov, A. A. (2004). Electric field effect in atomically thin carbon films. *science*, *306*(5696), 666-669. https://doi.org/10.1126/science.1102896

Payne, M. C., Teter, M. P., Allan, D. C., Arias, T. A., & Joannopoulos, J. D. (1992). CASTEP 4.2 Academic version, licensed under the UKCP-MSI Agreement. *Reviews of Modern Physics, 64*, 1045-1097. https://doi.org/10.1103/RevModPhys.64.1045

Perdew, J. P., Burke, K., & Ernzerhof, M. (1996). Generalized gradient approximation made simple. *Physical Review Letters*, *77*(18), 3865 https://doi.org/10.1103/PhysRevLett.77.3865

Rout, C. S., Late, D. J., & Morgan, H. (Eds.). (2019). *Fundamentals and sensing applications of 2D materials*. Woodhead Publishing. http://dx.doi.org/10.1016/B978-0-08-102577-2.00005-1

Sang, D. K., Wen, B., Gao, S., Zeng, Y., Meng, F., Guo, Z., & Zhang, H. (2019). Electronic and optical properties of two-dimensional tellurene: from first-principles calculations. *Nanomaterials*, *9*(8), 1075 https://doi.org/10.3390/nano9081075

M Santhosh, N., Filipič, G., Kovacevic, E., Jagodar, A., Berndt, J., Strunskus, T., ... & Cvelbar, U. (2020). N-graphene nanowalls via plasma nitrogen incorporation and substitution: The experimental evidence. *Nano-micro letters*, *12*(1), 1-17. https://doi.org/10.1007/s40820-020-0395-5

Seyler, K. L., Rivera, P., Yu, H., Wilson, N. P., Ray, E. L., Mandrus, D. G., ..., & Xu, X. (2019). Signatures of moiré-trapped valley excitons in $MoSe_2/WSe_2$ heterobilayers. *Nature*, *567*(7746), 66-70. https://doi.org/10.1038/s41586-019-0957-1

Sholl, D. S., & Steckel, J. A. (2011). *Density functional theory: a practical introduction*. New York: John Wiley & Sons

Song, H. Y., & Lü, J. T. (2018). Single-site point defects in semimetal WTe_2: A density functional theory study. *AIP Advances*, *8*(12), 125323. https://doi.org/10.1063/1.5057723

Sung, D., Min, K. A., & Hong, S. (2019). Investigation of atomic and electronic properties of $2D-MoS_2/3D-GaN$ mixed-dimensional heterostructures. *Nanotechnology*, *30*(40), 404002. https://doi.org/10.1088/1361-6528/ab2c16

Tian, Y., Zhu, Z., Ge, Z., Sun, A., Zhang, Q., Huang, S., ... & Meng, J. (2020). Electronic and magnetic properties of 3d transition metal doped $MoSe_2$ monolayer. *Physica E: Low-dimensional Systems and Nanostructures*, *116*, 113745. https://doi.org/10.1016/j.physe.2019.113745

Tongay, S., Suh, J., Ataca, C., Fan, W., Luce, A., Kang, J. S., ... & Wu, J. (2013). Defects activated photoluminescence in two-dimensional semiconductors: interplay between bound, charged and free excitons. *Scientific reports*, *3*(1), 1-5. https://doi.org/10.1038/srep02657

Tongay, S., Zhou, J., Ataca, C., Lo, K., Matthews, T. S., Li, J., ... & Wu, J. (2012). Thermally driven crossover from indirect toward direct bandgap in 2D semiconductors: $MoSe_2$ versus MoS_2. *Nano letters*, *12*(11), 5576-5580. https://doi.org/10.1021/nl302584w

Tonndorf, P., Schmidt, R., Böttger, P., Zhang, X., Börner, J., Liebig, A., ... & Bratschitsch, R. (2013). Photoluminescence emission and Raman response of monolayer MoS_2, MoSe2, and WSe_2. *Optics express*, *21*(4), 4908-4916. https://doi.org/10.1364/OE.21.004908

Tsumura, A., Koezuka, H., & Ando, T. J. A. P. L. (1986). Macromolecular electronic device: Field-effect transistor with a polythiophene thin film. *Applied Physics Letters*, *49*(18), 1210-1212. https://doi.org/10.1063/1.97417

Urbanová, V., Antonatos, N., Plutnar, J., Lazar, P., Michalička, J., Otyepka, M., ... & Pumera, M. (2021). Rhenium Doping of Layered Transition-Metal Diselenides Triggers Enhancement of Photoelectrochemical Activity. *ACS nano*, *15*(2), 2374-2385. https://doi.org/10.1021/acsnano.0c04437

Vargas-Bernal, R. (2019). Electrical properties of two-dimensional materials used in gas sensors. *Sensors*, *19*(6), 1295. https://doi.org/10.3390/s19061295

Wang, Y., Li, S., & Yi, J. (2016). Electronic and magnetic properties of Co doped MoS$_2$ monolayer. *Scientific reports*, *6*(1), 1-9 https://doi.org/10.1038/srep24153

Wang, Z., Carniato, F., Xie, Y., Huang, Y., Li, Y., He, S., ..., & Gianneschi, N. C. (2017). High relaxivity gadolinium-polydopamine nanoparticles. *Small*, *13*(43), 1701830. https://doi.org/10.1002/smll.201701830

Weng, Q., Li, G., Feng, X., Nielsch, K., Golberg, D., & Schmidt, O. G. (2018). Electronic and optical properties of 2D materials constructed from light atoms. *Advanced Materials*, *30*(46), 1801600 https://doi.org/10.1002/adma.201801600

Wu, J., Ma, X., Chen, J., & Jiang, X. (2019). Defects coupling impacts on mono-layer WSe$_2$ tunneling field-effect transistors. *Applied Physics Express*, *12*(3), 034001. http://doi.org/10.7567/1882-0786/ab00ea

Xin, Q., Zhao, X., & Wang, T. (2017). Electronic and magnetic properties of Mn-doped WSe$_2$ monolayer under strain. *Physica E: Low-dimensional Systems and Nanostructures*, *88*, 11-17. https://doi.org/10.1016/j.physe.2016.11.020

Yang, D., Fan, X., Zhang, F., Hu, Y., & Luo, Z. (2019). Electronic and magnetic properties of defected monolayer WSe$_2$ with vacancies. *Nanoscale research letters*, *14*(1), 1-9. https://doi.org/10.1186/s11671-019-3002-2

Yang, F., & Wu, M. W. (2016). Spin diffusion in p-type bilayer WSe$_2$. *Physical Review B*, *93*(23), 235433. https://doi.org/10.1103/PhysRevB.93.235433

Yazyev, O. V. (2010). Emergence of magnetism in graphene materials and nanostructures. *Reports on Progress in Physics*, *73*(5), 056501 http://dx.doi.org/10.1103/PhysRevB.77.193410

Ye, J., An, Y., Yan, H., & Liu, J. (2019). Defects and strain engineering the electronic structure and magnetic properties of monolayer WSe$_2$ for 2D spintronic device. *Applied Surface Science*, *497*, 143788. http://dx.doi.org/10.1016/j.apsusc.2019.143788

You, S., Yang, G., Li, C., Bi, M., & Fan, B. (2018, January).The wavefront compensation of free space optics utilizing micro corner-cube-reflector arrays [conference paper]. In *2017 International Conference on Optical Instruments and Technology: Optoelectronic Devices and Optical Signal Processings* (v. 10617, p. 1061709). Beijing: International Society for Optics and Photonics (SPIE). https://doi.org/10.1117/12.2295181

Yu, J., Li, Q., Liu, S., & Jaroniec, M. (2013). Ionic-liquid-assisted synthesis of uniform fluorinated B/C-codoped TiO2 nanocrystals and their enhanced visible-light photocatalytic activity. *Chemistry–A European Journal*, *19*(7), 2433-2441 http://dx.doi.org/10.1002/chem.201202778.

Zhang, J., Tian, P., Tang, T., Huang, G., Chen, X., Zeng, J., ... & Ji, Z. (2020). Ultrathin MoSe$_2$ three-dimensional nanospheres as high carriers transmission channel and full spectrum harvester toward excellent photocatalytic and photoelectrochemical performance. *International Journal of Hydrogen Energy*, *45*(11), 6519-6528. https://doi.org/10.1016/j.ijhydene.2019.12.217

Zhang, Y.,Chen, Y., Yang, F., Hu, S., Luo, Y., Dong, J., ... & Chen, Z. (2019). Sensitivity-enhanced fiber plasmonic sensor utilizing molybdenum disulfide nanosheets. *The Journal of Physical Chemistry C*, *123*(16), 10536-10543. https://doi.org/10.1021/acs.jpcc.9b00107

Zhou, Y., Su, Q., Wang, Z., Deng, H., & Zu, X. (2013). Controlling magnetism of MoS$_2$ sheets by embedding transition-metal atoms and applying strain. *Physical Chemistry Chemical Physics*, *15*(42), 18464-18470 https://doi.org/10.1039/C3CP52832D

Zhuang, H. L., & Hennig, R. G. (2013). Computational search for single-layer transition-metal dichalcogenide photocatalysts. *The Journal of Physical Chemistry C*, *117*(40), 20440-20445. https://doi.org/10.1021/jp405808a

UAE UNIVERSITY MASTER THESIS NO. 2022:22

The thesis describes the effects of band gap tuning of WSe_2 and $MoSe_2$ via vacancy creation and substitutional doping. Thesis discusses various configuration of vacancies, doping and their corresponding effects on the two compounds.

Shahida Maqsood received her Master of Science in Physics from the Department of Physics, College of Science United Arab Emirates University, UAE.

www.uaeu.ac.ae